ARMY RESEARCH LABORATORY

Vortex Ring Generator: Mechanical Engineering Design for 100-kpsi Operating Pressures

George K. Lucey, Jr.

ARL-TR-2096 January 2000

The findings in this report are not to be construed as an official Department of the Army position unless so designated by other authorized documents.

Citation of manufacturer's or trade names does not constitute an official endorsement or approval of the use thereof.

Destroy this report when it is no longer needed. Do not return it to the originator.

Army Research Laboratory

Adelphi, MD 20783-1197

ARL-TR-2096 January 2000

Vortex Ring Generator: Mechanical Engineering Design for 100-kpsi Operating Pressures

George K. Lucey, Jr.

Sensors and Electron Devices Directorate

Abstract

This report documents engineering design guidelines used to construct an explosive gas generator (100 kpsi maximum) and an adjustable area ratio (2844 maximum) nozzle. The equipment enables ring vortices to be generated using jet streams with significantly higher Mach numbers than previously reported in the literature. Studies are planned of the risks, limits, and capabilities of ring vortices for nonlethal crowd control applications. The focus is limited to 40-mm weapons, so this report is written to facilitate technology transfer to investigators interested in other applications and launch platforms.

Contents

Figures

Tables

1. Introduction

The Army Research Laboratory was tasked by the USMC Joint Non-Lethal Weapons Directorate to investigate vortex rings as a means of large-area crowd control. The goals were to apply knockdown impulses at close range and to transport disabling irritants to more distant targets. The universal vortex ring generator (VRG) shown in figure 1 was constructed to study the internal ballistic parameters critical to control for optimum vortex range and target effects. This report presents the mechanical design and safety tests as well as the vortex research, which includes both simulation studies and live-fire experiments. Unique design features are a variable gas generator and an adjustable supersonic nozzle. These features enable an operator to quickly tailor an explosive pressure-time pulse (100 kpsi maximum) and generate different diameter jet streams (10 in. maximum) at high Mach numbers without a Mach disk at the muzzle.

The hardware was designed around the flow patterns of the MK19-3 automatic 40-mm grenade launcher, and figure 2 shows the first image of a vortex from a weapon of this size. The image was generated by initiating a small detonator in the breech of a 40-mm barrel.

Audiovisual recordings taken during safety field tests of larger explosive charges showed the performance in the as-built condition (without any optimization effort) to be as follows: 2-ft-diam vortices knocking down a 150-lb mannequin at 30 ft (see fig. 3), a 125-lb mannequin at 40 ft, and a 75-lb mannequin at 50 ft. The vortex also transported chalk dust 50 ft, and the average velocity measured at a target 120 ft downrange was 160 ft/s. Well-formed vortices from smokeless powder were not visible and had the whistle of incoming artillery.

The machine gun application was removed as a USMC Joint Non-Lethal Weapons Directorate program and returned to Technology-Base research in CY 1999 in an effort to improve the range from 100 to 300 m. Design guidelines that were followed in constructing the prototype hardware are presented herein in part as a final report for the nonlethal program, and in part to facilitate technology transfer to other platforms and applications, such as the GL6 repeating 40-mm revolver for nonlethal close-quarters crowd control.

Each component in the variable gas generator and the adjustable nozzle is addressed in the following sections from a mechanical engineering viewpoint. For example, dimensions and materials needed by the machine shop to fabricate first prototype hardware for field test are defined using approximate theory of plasticity limit analyses. The transient flow of burning propellant is treated using standard rocket engine analyses. In addition, the mechanisms of vortex formation at high Mach numbers are treated using computational fluid dynamics analyses of cylindrical gas slugs. No effort was made at precision calculations or vortex parameter measurements. The goal was to overdesign the hardware to ensure safety while producing a product that could be refined in field test.

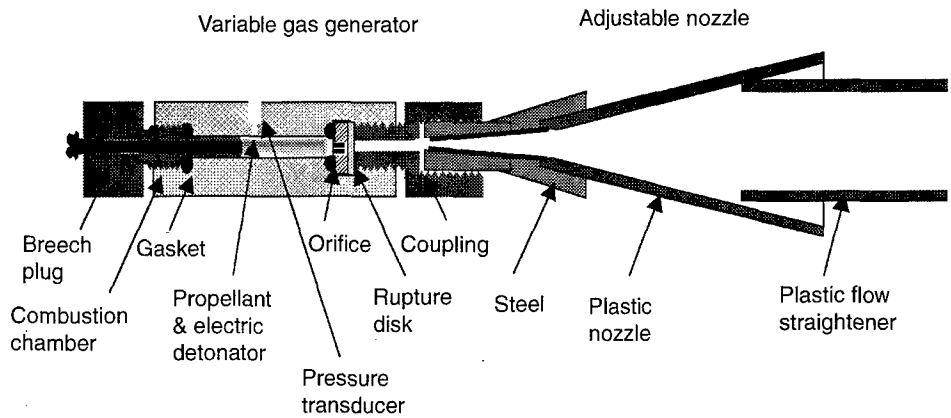

Figure 1. Assembly view of the universal vortex ring generator.

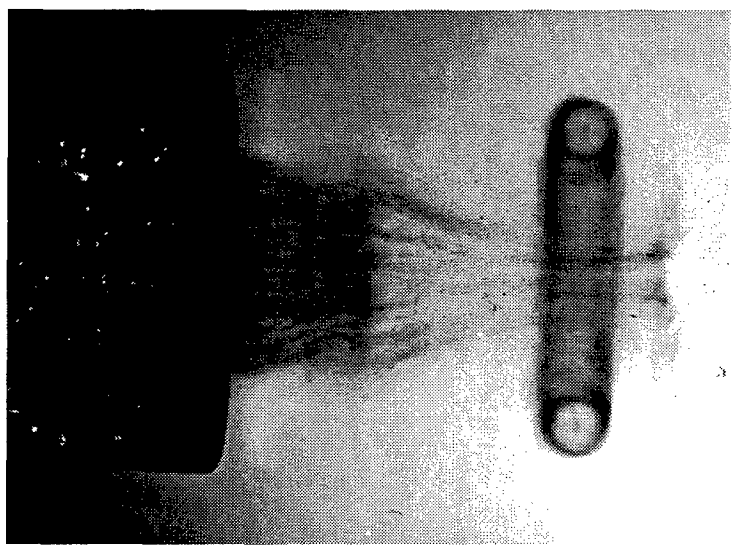

Figure 2. Shadow graph of a low-energy, 40-mm vortex ring (courtesy D. Lyons, Aberdeen Proving Ground).

Figure 3. Vortex ring knockdown of a 150-lb mannequin at 30 ft.

To inquire about videos and soundtracks on CD, contact glucey@erols.com.

2. Variable Gas Generator

The gas generator, shown in figure 4, is used to form a tailored pressure pulse at the throat of the vortex ring gun nozzle by electrical initiation of a powder propellant. The assembly consists of a thick-walled combustion chamber with a port for a pressure transducer, a threaded base plug for breech loading prepackaged explosives, and a threaded coupling for attaching an orifice to a diverging nozzle. The operator can tailor the shape of the pressure pulse from shot to shot by loading different types and weights of explosives, altering the combustion chamber free volume, and changing the size of the orifice that controls the mass flow rate into the nozzle.

The safe operating pressure signatures within which the gas generator is designed to operate are shown in table 1. The baseline pulse shape in this performance specification represents the internal ballistics of the stockpile M385 practice round used in the MK19-3 automatic 40-mm grenade launcher, and the upper limit was arbitrarily selected.

The mechanical configuration selected for the gas generator is designed for safe and flexible vortex ring research in a field environment and is not intended to represent a weapon proposed for general issue to the soldier. The engineering analyses used to define the materials and dimensions needed by the machine shop to manufacture the hardware are presented in the following sections. Reliance was placed upon theory of plasticity and limit analyses equations rather than finite element modeling so that quick redesigns could be machined during actual field tests without compromising safety. The equations may be used in future studies to scale the gas generator to larger or smaller platforms.

Figure 4. Assembly view of gas generator.

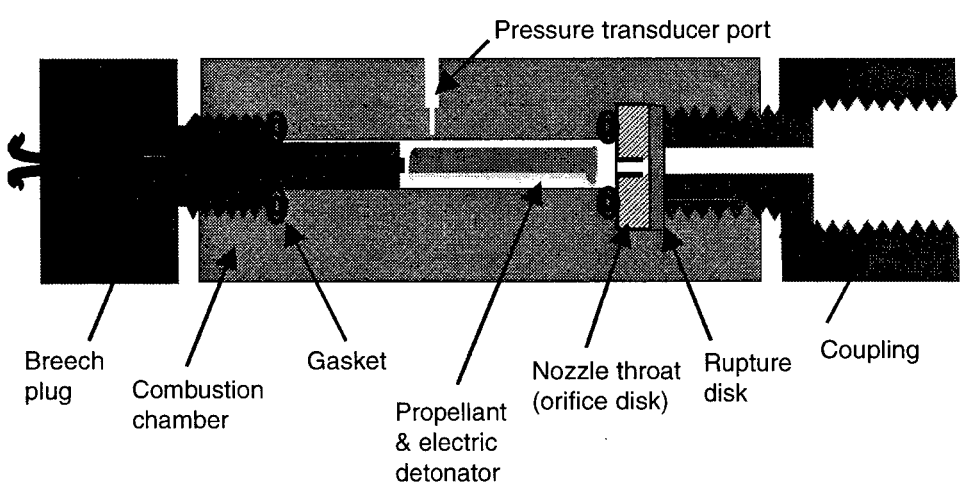

Table 1. Gas generator performance specifications.

33,000 psi	< Pressure	<	100,000 psi
1.5 ms	< Duration	<	7.5 ms
0.01 lb	< Weight	<	0.05 lb

2.1 Combustion Chamber Design

Whether the analysis is by computer modeling or plasticity limit equations, the technology gaps are common to both. In short, a detonation subjects the materials to multiaxial strains and temperatures at high rates of loading, and no literature exists that lists the physical properties of materials subjected to these combined loads.

Material properties cataloged in the literature are generally measured from loads applied along a single axis. To use these data in the design of structures in multiaxial loading, an effective uniaxial stress must be calculated. Different theories are available for calculating the effective uniaxial stress in different materials, and Faupel has shown that octahedral shearing stress theory appropriately predicts failure in steel combustion chambers (Faupel, 1964, pp 589–593). (See example in fig. 5.) In this instance, bursting under a static pressure load is defined by

$$P_{\text{burst}} = \frac{2\sigma_y}{k\sqrt{3}}\left[\ln\frac{d_o}{d_i}\right]\left(2-\frac{\sigma_y}{k\sigma_u}\right), \tag{1}$$

where

σ_y = yield stress, psi,
σ_u = ultimate stress, psi,
d_o = outer diameter, in.,
d_i = inner diameter, in.,
k = stress concentration factor, and
P_{burst} = burst pressure, psi.

When the pressure is transient rather than steady, inertia must be taken into account during stress calculations. The concern is to avoid stress magnifications that occur when the pulse duration is within ±50 percent of the natural period. On the other hand, if the pulse duration is less than 25 percent of the natural period, then the force felt during a detonation is attenuated and a larger dynamic pressure can be sustained by the chamber:

$$P_{\text{dynamic}} = P_{\text{burst}}\left(1+\frac{\tau_n/4}{t}\right) \tag{2}$$

$$\tau_n = \pi\left\{\frac{d_o+d_i}{\sqrt{E/\rho}}\right\}, \tag{3}$$

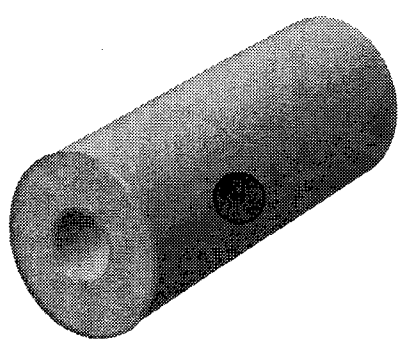

Figure 5. Thick-walled combustion chamber with side hole for pressure transducer.

where

τ_n = natural period, s,
E = modulus of elasticity, psi,
ρ = density, lb-s^2/in.^{4}, and
t = duration of applied force, s.

These equations ignore the axial stresses caused by end loading of the combustion chamber, but Faupel showed that they were reasonably good predictors of failure in pipe bombs made of 1020 steel. Therefore, they were selected to design the vortex gas generator from a stronger 4000-series steel.

Typical uniaxial properties for heat-treated 4000-series steel are listed in table 2. We used a wide range of strengthening heat treatments as the basis for selection for the gas generator application. The 4340 steel is preferred, but often less available at local suppliers. The 4140 is the backup selection used in most testing at ARL, and the more moderate ductilities were generally specified for the prototype gas generator to avoid sudden brittle fractures in field operations.

If a pressure transducer is mounted in the chamber wall, then the localized stress concentration factor from the side hole is

$$k = 2.5 \tag{4}$$

(Faupel, 1964, pp 648, 752).

Substituting this value and the properties of tempered 4340 steel into the burst pressure equation (1) defines the wide range in combustion chamber diameters in table 3 that can sustain a pressure of 100 kpsi.

Table 2. Mechanical properties of 4000-series steels (Tapley, 1990).

Material	Treatment	Hardness Bhn (Rc)	Elongation (%)	Yield stress (kpsi)	Tensile stress (kpsi)	Elasticity modulus (mpsi)	Density (lb-s^2/in.^{4} $\times 10^{-6}$)
4340 steel, Ni-Cr-Mo	Tempered 1200 °F	280 (29)	19	124	140	28	725
	Normalized 1650 °F	363 (39)	12	125	185	28	725
4140 steel, Cr-Mo	Tempered 1200 °F	230 (20)	22	95	110	28	725
	Normalized 1650 °F	302 (32)	18	95	148	28	725

Table 3. Burst conditions for a 4340 steel cylinder with a side hole (k = 2.5) subjected to 100 kpsi.

Inner diam d_i (in.)	Outer diam d_o (in.)	Natural period (1/s)
0.25	0.72	0.000016
0.50	1.44	0.000031
0.75	2.17	0.000047
0.875	2.53	0.000054
1.00	2.89	0.000062
1.25	3.61	0.000078
1.50	4.33	0.000093

The dimensional relationship for these conditions is linear:

$$d_o \sim 3\, d_i . \tag{5}$$

Since the gas generator is being patterned after flow in the MK19-3 gun, the 7/8-in. diam of the spherical combustion chamber in the M385 practice round is selected as the inner diameter for the VRG combustion chamber.

The outer diameter is shown in table 4 for two tempered steels.

These calculations suggest that 1 in. should be added to the diameter of the combustion chamber if the material is changed from 4340 to 4140 steel. A decision was made instead to use a standard 3-in. rod made from either steel, and the weaker 4140 was selected for field trials due to availability. The logic was that the materials were not brittle and would not experience catastrophic failure. The rods were to be monitored for flatness from shot to shot and removed if diameters exceeded a 5-percent strain.

Concern over stress amplification exists due to the explosive pulse being in resonance with the dimensions selected for the cylinder. The previous calculation showed that the natural period in the radial mode was 0.06 ms and the range of specified explosive pulses was 1.5 to 7.5 ms; therefore, the impulsive loading is essentially static and radial inertia effects may be ignored. Figure 6 shows the final combustion chamber design.

During early phases of the vortex program, combustion chambers were made without breech plugs from both 4340 and 4140. Roughly 100 safety test shots were conducted over a wide range of explosive charges, the maximum charge being 25 g of fast-burning, smokeless powder initiated by 1 g of HMX high explosive. Many peak pressure spikes approached

Table 4. Combustion chamber diameters for two steels.

d_i (in.)	Material	d_o (in.)
7/8	4340 tempered	2.5
7/8	4140 tempered	3.5

Figure 6. Combustion chamber design.

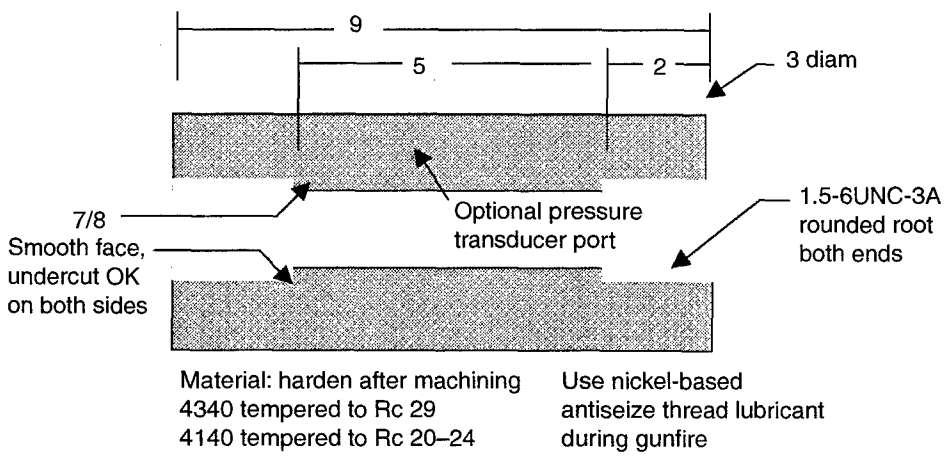

125,000 psi, and since there was no evidence of external bulging, the design was released for use in field research.

2.2 Breech Plug Design

The breech plug is used for confining high pressures, reloading propellant packages after each shot, accessing wires from the electric initiator, and altering the free volume in the combustion chamber by the insertion of a shaft chosen from a variety of available lengths. Figure 7 is a diagram of the gas generator breech plug. Operation of the breech plug must be quick and safe, and this requires that the threads remain elastic when exposed to high-pressure pulses. Even small inelastic deformations may result in jamming that is not only difficult and time-consuming to remove, but also requires both tap and die touchup for reassembly. To minimize jamming and gas leakage, a standard Unified National Coarse (UNC) thread is specified, the plug diameter is made larger than the combustion chamber, and an optional copper gasket is used to restrict the area of high-pressure gas exposure. Selection of the length and size of thread is determined by equating the axial force generated by pressure in the combustion chamber to the shearing force in the threads, and then referring to the literature to determine the area within the threads upon which the shearing stresses are assumed to act.

The diagram in figure 7 illustrates the relationship between the axial force and the shearing force; this relationship is further expressed by

$$\text{shear force} = \text{axial force} \ ,$$

$$\tau_y A_s = PA \ , \tag{6}$$

where

$\tau_y = \sigma_y/2$ = shear yield stress, psi,
σ_y = tensile yield stress, psi, and
A_s = thread area in shear, in.^{2};

$$A_s = L_e \, \pi \, n \, K_n \left[\frac{1}{2n} + 0.577\left(E_s - K_n\right) \right] = L_e \lambda \ , \tag{7}$$

where

L_e = length of thread engaged, in.,
n = threads per inch,
K_n = minor diameter of threaded hole, in.,
E_s = plug thread pitch diameter, in.,
$A = \pi d^2/4$ = plug area exposed to gas, in.^{2}, and
P = combustion chamber pressure, psi.

Equations (6) and (7) show

$$L_e = \frac{\pi P d_i^2}{2 \sigma_y \lambda} \ . \tag{8}$$

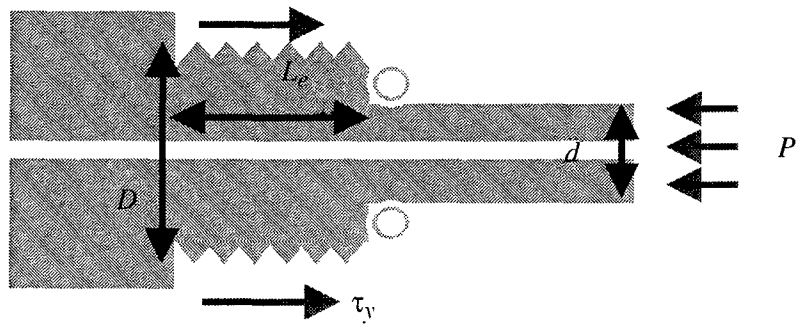

Figure 7. Free-body diagram of gas generator breech plug.

Values for the thread constants shown in table 5 were obtained from Green (1996).

Substituting various shaft diameters into the shear area equation (7) provides the listing in table 6, wherein λ is seen to be a linear function of diameter ($\lambda \sim 2.15$ D).

Substituting the approximation for λ provides a simplified expression for thread length:

$$L_e \approx 0.73 \left(\frac{P}{\sigma_y} \frac{d^2}{D} \right) . \tag{9}$$

If the breech plug gasket provides a good seal, then the propellant pressure acts only across the 0.86-in. shaft protruding into the combustion chamber. If the gasket is missing or leaks, then the pressure acts over the major diameter of the breech plug thread, D. Both situations are analyzed

Table 5. Standard bolt properties.

D, shaft major diam (in.)	n, shaft (threads/ in.)	E_s, shaft pitch diam (in.)	K_n, hole minor diam (in.)
3.0	4	2.84	2.73
2.5	4	2.34	2.23
2.0	4.5	1.86	1.76
1.5	6	1.39	1.32
1.25	7	1.16	1.09
1.0	8	0.92	0.86

Table 6. Effective shear areas of standard bolts.

D, bolt major diam (in.)	$A_s/L_e = \lambda$, shear area/ engaged length
3.0	6.43
2.5	5.25
2.0	4.14
1.5	3.11
1.25	2.58
1.0	2.03

in this report, and as a starting point, a standard thread larger than 1 in. was arbitrarily selected, namely,

$$D = 1.5 \text{ in.}, 6 \text{ threads/in.} \quad (10)$$

The length of threads needed for this diameter shaft is calculated in table 7 for two types of steel.

Experience has shown that shearing stresses in bolts do not distribute uniformly, and the first three to four threads could bear four times more loading than the following threads. To comply with good design practice, the length of thread selected for prototype field testing was doubled:

$$L_e = 2.0 \text{ in.} \quad (11)$$

(Blake, 1986).

A schematic of the recommended base plug is shown in figure 8. This design has only been test fired 10 times because all previous combustion chambers were muzzle-loading designs and breech plugs were not used. The tests were performed at 75 kpsi without copper gaskets. The design was shown to be safe and free of jamming tendencies.

Table 7. Breech plug engagement requirements for different seals and materials.

Material	Good seal	Leaky seal
4340 tempered to Rc 29	$L_e \sim 0.3$ in. $n \sim 2$ turns	$L_e \sim 0.9$ in. $n \sim 5$ turns
4140 tempered to Rc 20	$L_e \sim 0.4$ in. $n \sim 2$ turns	$L_e \sim 1.1$ in. $n \sim 6$ turns

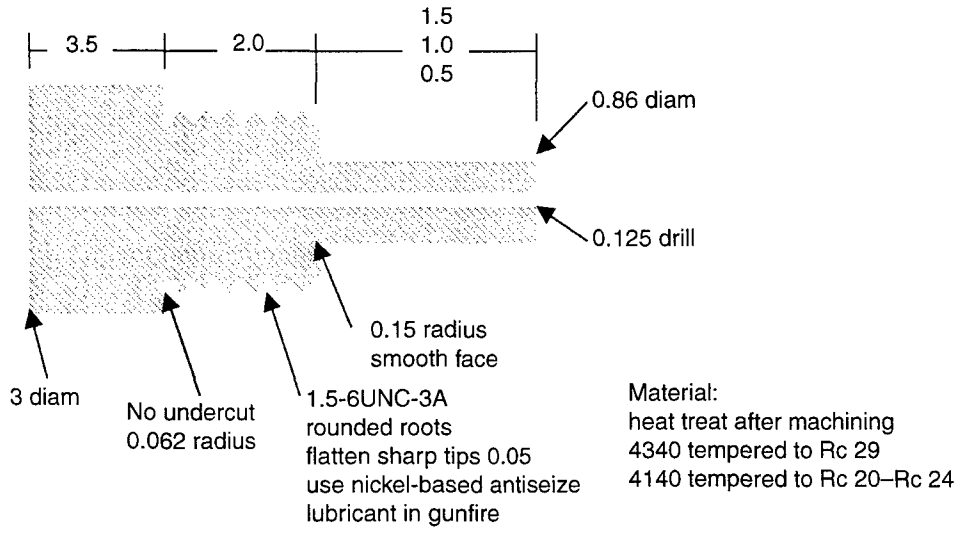

Figure 8. Breech plug design.

2.3 Coupling Design

The nozzle coupling is an interface between the combustion chamber and the supersonic nozzle. Unscrewing the coupling from the combustion chamber enables quick changes in the rupture disk if necessary to improve powder initiation in the combustion chamber. The coupling also provides quick access to the nozzle orifice disk if gas erosion damages the shape and size, or if a different throat diameter is required to adjust the mass flow rate. Finally, the coupling allows muzzle loading as an alternative to breech loading.

The coupling must be designed for propellant flow rates less than, equal to, and greater than the rate for the MK19-3 when firing blank cartridges. The blank selected as the standard for this program is the M169 cartridge used in the M385 practice round. The cartridge has a series of six exhaust ports equivalent in area to a ¼-in. hole, so the decision was made to configure the gas generator with removable orifices having throat areas equal to, greater than, and smaller than the M169, i.e., ¼, ½, 3⁄16 in.

To accommodate the largest orifice, the coupling diameter must be ½ in. or more. Figure 9 shows the assembly of a small orifice onto a threaded coupling with a ½-in. bore. The analytical tasks are to estimate the outer diameter, thread size, and length of thread that will confine the internal shaft pressure without jamming. Two concerns are inelastic axial and radial strains, and these are discussed below. A technology gap exists in that the radial analysis must address small deformations on the order of tolerances between mating threads, and such calculations are unreliable for elastic-perfectly-plastic materials. We use a semiempirical approach to address this problem, specifically to estimate safe dimensions and then conduct refinements through field tests.

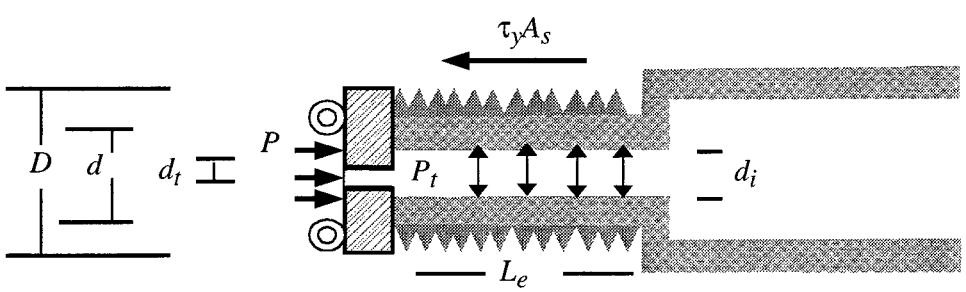

Figure 9. Free-body diagram of the gas generator coupling assembly.

$\tau_y = \sigma_y/2$ = shear yield stress, psi,
σ_y = tensile yield, psi,
$A_s = L_e\lambda$ = thread area in shear, in.^{2},
L_e = length of thread engaged, in.,
λ = thread constant, in. (table 5),
D = major thread diameter, in.,
d_i = hole diameter, in.,
d_t = orifice diameter, in.,
d = internal gasket diameter, in.,
P = combustion chamber pressure, psi, and
P_t = throat pressure, psi.

If the assumption is made that gas flowing through the orifice is critical (i.e., Mach 1), steady, isentropic, and adiabatic, then the pressure along the length of the coupling shaft may be approximated by (Sutton, 1992, p 52)

$$P_t = P\left[\frac{2}{\gamma+1}\right]^{\gamma/(\gamma-1)}, \tag{12}$$

where

γ = ratio of propellant-specific heats.

A value for the specific heat ratio was obtained from Primex Industries for WAA90 smokeless powder:

$$\gamma = 1.226 . \tag{13}$$

Substituting shows

$$P_t = P(0.56) . \tag{14}$$

Equation (1) defines the dimensions of smooth cylinders required for an internal pressure to develop full yielding. The coupling shaft is not smooth, however, but has a helical notch along the surface. A stress concentration factor for multiaxial loading was not found in the literature, so engineering experience led us to the assumption that $k \sim 2.5$ for threads with rounded roots. For a stagnation pressure of 100 kpsi, the coupling shaft pressure is then 56 kpsi, and the shaft diameters, D, which become completely inelastic, are shown in table 8 for two steels.

We performed many field tests using a 1-8UNC-3A threaded shaft made from 4140 tempered steel and drilled to a ½-in. entrance diameter. In these tests, the orifice was not located at the entrance to the coupling; therefore, the inner diameter was exposed to the full combustion chamber pressure. Slight jamming resulted under pressures of 50 to 60 kpsi. The first few threads distorted and required die rework after each firing. Internal threads never distorted, but tap rework was often required for cleaning propellant residue. Severe jamming always resulted at 100 kpsi.

We drew the following conclusions from these tests: (1) the design guidelines, based upon an assumed stress concentration factor of $k = 2.5$, appear to be reasonable; (2) the orifice must be at the front of the shaft to serve as a pressure reducer; and (3) a larger diameter and stronger thread are needed to avoid rework after each shot.

Table 8. Failure dimensions for coupling shafts made from two steels.

d_i (in.)	Material	D (in.)
0.500	4140 Rc 20	1.08
0.500	4340 Rc 29	0.91

An interim selection is shown in figure 10. We made prototype couplings to these new dimensions using 4140 tempered steel, but there have only been 10 test firings. Field tests showed the design to be safe, but operations above 70 kpsi continued to show jamming tendencies. We recommend using 4340 Rc 29 steel, reducing the 0.5-in. drill size, and redesigning for a stronger buttress thread.

2.4 Prepackaged Explosives

All propellant and detonator applications proposed for vortex studies are reviewed by a safety officer, and all handling, packaging, firing, and disposal of explosives is performed by a weapons officer. Loading is conducted in an area certified for explosives, and firing of untested hardware takes place at a remote ballistics test range. Hardware proven safe is tested to Occupational Safety and Health Administration (OSHA) acoustic standards, and an environmental impact review is performed before operational test firings are conducted. Field research is performed in a fenced test range with the combustion chamber mounted inside a protective metal enclosure, as shown in figure 11. Use of the equipment and explosive loading described in this report is not recommended without similar safety controls. OSHA standards require the use of earplugs for single-shot firing of the vortex ring generator. The program did not use rapid fire at this stage of development, so the acoustics were not measured and ear protection was not defined.

Both muzzle and breech loadings are used to charge the gas generator. Muzzle loading uses a combustion chamber open on one end only, i.e., no breech plug. The assembly is structurally stronger and therefore safer for testing unproven hardware. After each shot, the generator is disassembled, failures are analyzed, and either redesigns or repairs are made. Propellant is then reloaded and the gun is returned to the firing site. The focus is on data gathering for hardware performance, not vortex generation, and the average for a four to five man crew is six to eight shots a day. The change to breech-loading hardware halves the crew size and

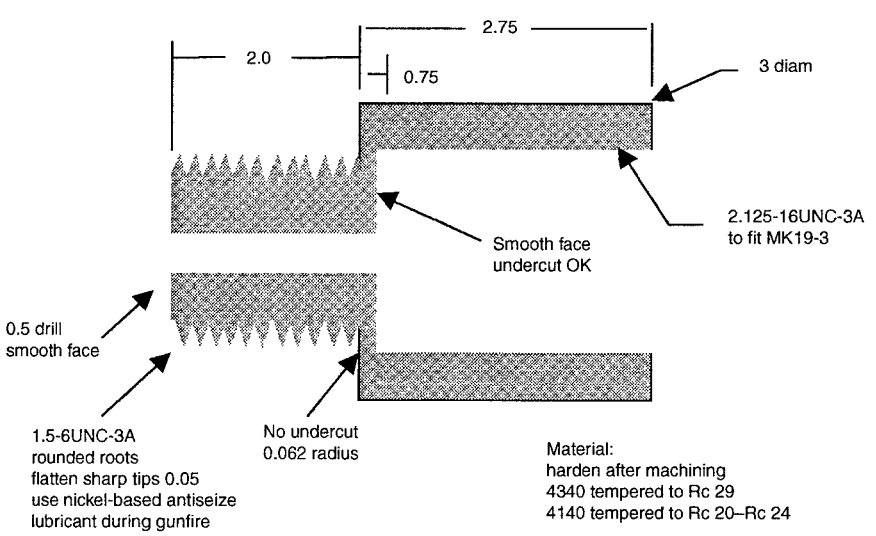

Figure 10. Coupling design.

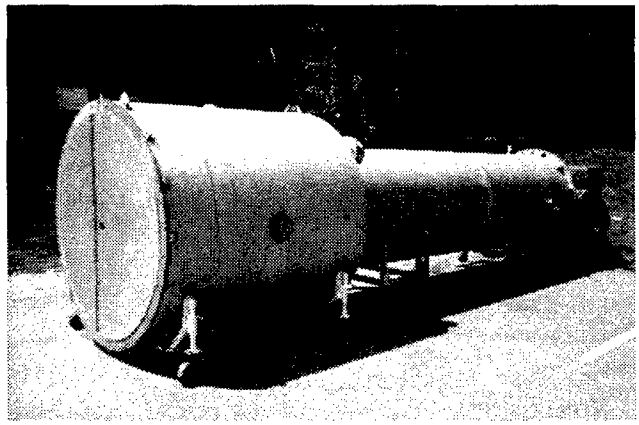

Figure 11. Environmental chamber for firing agent-laden vortex rings.

triples the rate of fire, thereby facilitating future operations aimed at data gathering on vortex propagation and target effects.

Because Winchester WST1 smokeless powder and the Navy MK17 electric squib initiator were readily available, we used them to perform most of the safety and operational testing. Pressure transducer data to be described later showed that the wide range in pressure signatures specified for the gas generator was indeed achieved. Videos of the muzzle blast, however, showed significant propellant burning outside the gun that worsened as the diameter of the nozzle orifice increased.

Since external burning is a source of turbulence perceived to degrade the formation of vortices, we made cursory inquiries into the significance of a rupture disk, type of initiator, position of the initiator, orientation of the initiator, and type of propellant. Conclusions were drawn that a faster-burning propellant and more powerful detonator would significantly reduce external burn.

C4 high explosive was tried and discarded as a propellant. This is because the structural integrity of the combustion chamber is limited to C4 charges below 8 g, and although the resulting exhaust gas velocity is high, the momentum of the vortex is low. Heavier propellants are needed for target knockdown, and candidates available at a local gun shop were Red Dot, Bulls Eye, and HiSkor smokeless, fast-burning powder. Charges up to 30 g can be prepackaged and combined with high-explosive electric initiators to optimize burn.

The combination that proved to be the most reliable in approximately 50 firings was Red Dot fast-burning, smokeless powder initiated by a Reynolds RP83 electric detonator containing 1 g of HMX high explosive. Figure 12 shows that commercial cardboard tubing, tape, foam, and glue can be used to prepackage an inventory of different explosive firecrackers of different lengths. This packaging enables an operator to tailor pressure pulses and flow rates by mixing and matching explosives, breech plugs, and nozzle orifices.

To analyze stress distributions and fluid flow, the properties of gasses generated in the combustion chamber must be obtained from powder manufacturers. Primex Industries proved to be most cooperative and provided the data in tables 9(a) and (b) from their existing library for

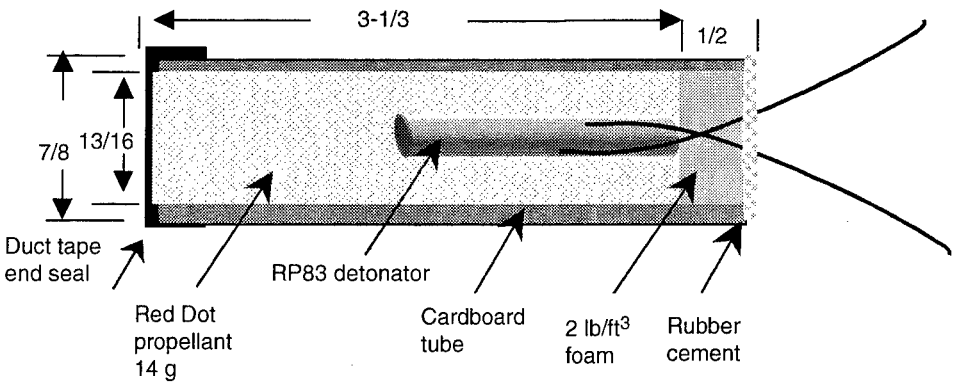

Figure 12. Prepackaging technique for the vortex ring propellant and electric detonator.

Table 9 (a). Combustion properties of WAA90 propellant (courtesy Primex Industries).

Density (g/cm^3)	Pressure (MPa)	Temp (K)	Mol Wt	Co-Volume (cm^3/g)	Frozen gamma, γ
0.035	38.600	3218	25.2	1.061	1.226
0.040	44.400	3222	25.2	1.060	1.226
0.045	50.260	3226	25.2	1.058	1.226
0.050	56.200	3229	25.2	1.056	1.226
0.055	62.200	3232	25.2	1.054	1.226
0.060	68.260	3234	25.2	1.052	1.226
0.065	74.400	3237	25.2	1.050	1.226
0.070	80.610	3239	25.2	1.048	1.226
0.075	86.880	3241	25.2	1.046	1.226
0.080	93.220	3242	25.2	1.045	1.226

Table 9 (b). Assumed properties of WAA90 obtained from other sources.

Property	Value	Unit
Universal gas constant	8314	MPa/(kmol-K)
Gas constant	330	MPa/(kmol-K)
Density	326.6	J/K-kg
Dynamic viscosity	0.0000185	kg/s-m
Specific heat	1801.8	J/kg-K
Thermal conductivity	0.0262	W/m-K
Expansion coefficient	0.0033	1/K

WAA90 and other smokeless powders. Listings were more difficult to obtain from other manufacturers without purchasing new testing. Since the vortex program is in the early stages of hardware design, the assumption is made that the Primex listings are representative of the more energetic Red Dot, HiSkor, and Bulls Eye powders also used in field testing.

2.5 Rupture Disk Design

Rupture disks are used to seal explosives from the environment and also to increase the rate of propellant burn by raising the combustion chamber pressure. A literature search was not performed, so design equations were not available to assist in the selection of a material and thickness for the gas generator application. In an effort to derive an equation, we examined an expended M169 cartridge microscopically, and this showed that the rupture disk was often pushed through the exhaust port like a deep

drawing operation, as depicted in figure 13, rather than a shear punch. A proven expression for deep drawing force is

$$F = 4DTmK \ , \tag{15}$$

where

F = drawing force, lb,
d = punch diameter = $(D - 2T)$, in.,
D = disk diameter, in.,
T = disk thickness, in.,
K = shear strength, psi, and
m = material constant.

Values of the material properties K and m cited in equation (15) are provided for a few materials in table 10.

Linear interpolation shows an expression for the average value of m:

$$m = k(15.6 \times 10^{-6}) \ . \tag{16}$$

Rearranging equation (15) in terms of pressure and substituting for m gives

$$P \approx \frac{80 \times 10^{-6}\left(D\ T\ K^2\right)}{\left(D - 2T\right)^2} \ , \tag{17}$$

where

$$K = \frac{\text{ultimate tensile strength}}{2}, \text{psi} \ .$$

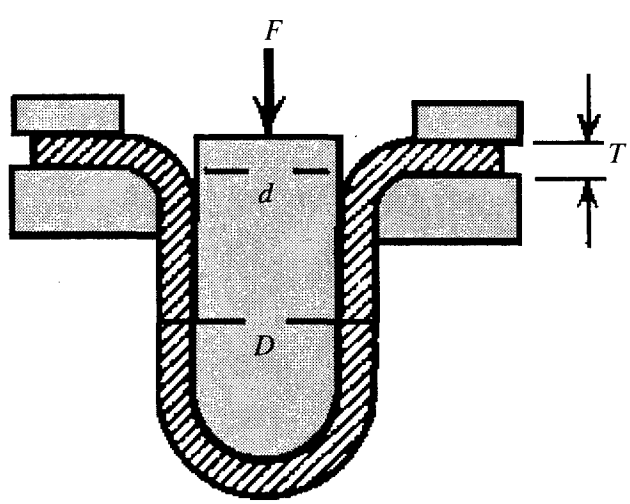

Figure 13. Deep draw operation.

Table 10. Drawing properties at the temperatures and forming rates in a foundry (Faupel, 1964, p 441).

Material	K (psi)	m	d/D limit
Nickel	75000	1.00	0.55
Mild steel	50000	0.86	0.60
Brass	40000	0.60	0.70
Copper	30000	0.40	0.80

The value of K generally applies to low strain rates and thermal gradients. Because this is not the case with explosive forming in rupture disks, we used a trial calculation on the rupture disk in the M169 cartridge to perform a sort of "reality check."

The M169 cartridge uses a brass foil to cover six exhaust ports as shown in figure 14. The shear strength is half the average tensile strength, $K \sim 18{,}000$ psi; therefore, the coupling coefficient is calculated from equation (15) as $m = 0.28$. Substituting into equation (16) shows that the pressure to rupture is $P = 3159$ psi. This is judged to be within the realm of possibility since M2 propellant in the cartridge achieves a higher peak pressure of 32 kpsi (Baxivanos, n.d.).

The operator of the gas generator has three orifice diameters to choose from (namely, ¼, ½, and 3⁄16 in.), and a different rupture disk thickness is required for each if the mounting is the same as in the M169 cartridge. To avoid this situation, the rupture disk is placed behind the orifice over the ½-in. coupling exhaust port, as shown in figure 15.

In this position, a universal rupture disk accommodates all three nozzle throats. See figure 16.

If we assume that (1) all the fast-burn, smokeless propellants used in the gas generator require the same release pressure as the M2 propellant, and that (2) the same brass material is used to machine the rupture disk, then equation (16) shows that the foil thickness over a ½-in. hole should be 50 mils.

This guideline became the basis for a field test aimed at refining the rupture disk design. The firing conditions were as follows: use of a Navy M17 electric squib initiator, 12-g Winchester WST1 powder, no empty volume in the combustion chamber other than free space between powder grains, a 3⁄16-in. orifice, and a ½-in. coupling exhaust port. Four rupture disks were tested:

20-mil beryllium copper,
60-mil beryllium copper (three 20-mil disks),
32-mil spring steel, and
10-mil fish paper (i.e., waxed cardboard).

Pressure signatures measured at the rear of the powder showed no discernable differences between strong and weak disks (~65-kpsi peak, ~5-ms duration). In fact, results with simple cardboard led us to conclude that a rupture disk was not needed and that its use could be eliminated.

We performed many field tests without rupture disks, and observed vortices to be generated. Repeatability was initially poor, however, and this was attributed to excessive propellant burn outside the combustion chamber. This hypothesis was somewhat validated when we used high-explosive detonators to initiate the powder rather than squibs, and reliability improved. At the time of this writing, the repeatability was 33 percent and additional design effort is needed. We are now considering restoring the rupture disk in the same thickness and mounting as originally designed in the M169 cartridge.

Figure 14. Cross-sectional view of M169 cartridge high-pressure chamber. (Picatinny Arsenal Drawings, 8886329 Case, Cartridge, 40-mm: M169, 9206911 Cup Closing, 886327 Cartridge Case Assembly 40-mm M169.)

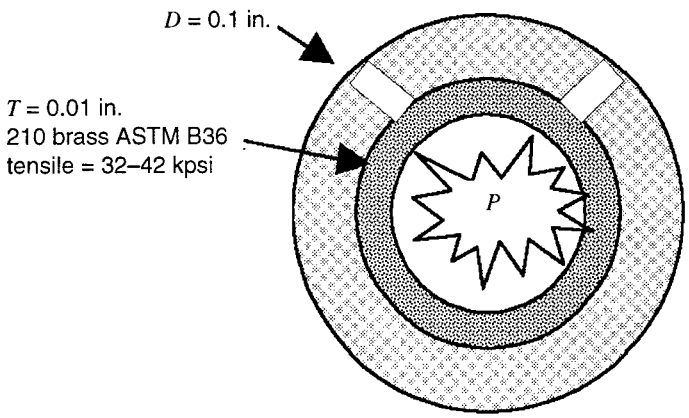

Figure 15. Proposed mounting of a rupture disk.

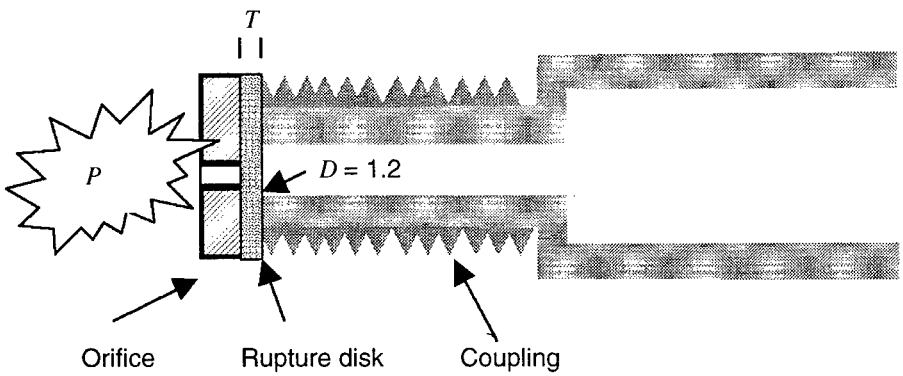

Figure 16. Front view of rupture disk showing pressure distribution to be approximately equal for all three sizes of orifice disk.

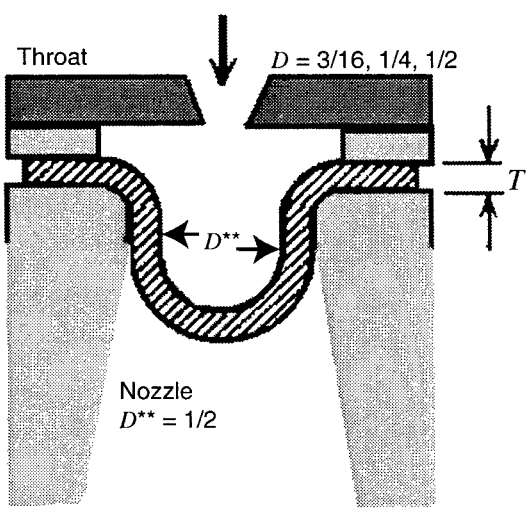

3. Adjustable Nozzle Design

The gas generator nozzle eliminates the Mach disk at the muzzle and emits high Mach-number jet streams by expanding the propellant in the combustion chamber to near atmospheric pressures. The task is to design a universal nozzle capable of operating over a very wide range of combustion chamber pressures without the need to stockpile a large inventory of hardware. The primary obstacle is the absence of convenient engineering design equations for a flow that is both unsteady and diabatic, i.e., involving the addition of heat by continued propellant burn outside the combustion chamber.

This report sorts the design problem into two categories: small fill (0 to 5 g) and large fill (10 to 30 g) in the combustion chamber. Nozzles for small charges are of interest to researchers who would like to scale down the vortex ring gun and perform studies that do not require five-man field test crews and special test ranges. Nozzles for larger charges are of interest to researchers who would like to optimize the range and target effects.

When the combustion chamber is nearly full, propellant flow momentarily reaches steady state, i.e., the blast shock departs the gun tube before the peak pressure at the back of the combustion chamber degrades. For this condition, textbook rocket engine equations based on isentropic, adiabatic, steady flow can be used to define the first iteration nozzle for field test. The effects of propellant burn inside the nozzle are simply left for field test; the expectation is that a longer nozzle could be required.

To simplify both design and fabrication, all prototypes are long diverging cones rather than short contoured configurations. In addition, the nozzles have a discontinuity in that the throat diameter is adjustable through orifice replacement. All flow analyses disregard the discontinuity and assume that flow through the throat is critical (Mach 1).

A generalized schematic is shown in figure 17, and for each orifice replacement to a smaller diameter, the flow is treated as though the cone length extends until $D^{**} = D^{*}$.

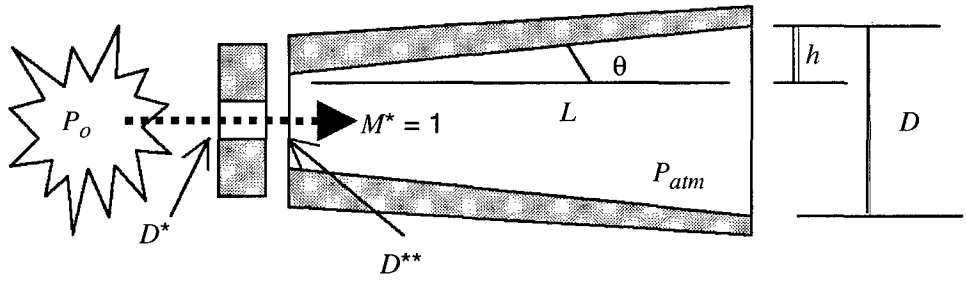

Figure 17. Adjustable nozzle design.

The diameter at which the flow exhausts at atmospheric pressure may then be calculated from

$$\left[\frac{D^*}{D}\right]^2 = \left[\frac{\gamma+1}{2}\right]^{1/(\gamma-1)} \left[\frac{P_{atm}}{P_0}\right]^{1/\gamma} \sqrt{\frac{\gamma+1}{\gamma-1}\left[1-\left(\frac{P_{atm}}{P_0}\right)^{(\gamma-1/\gamma)}\right]} \quad , \quad (18)$$

where

D^* = throat diameter, in.,
D = exit diameter, in.,
γ = ratio of propellant-specific heats,
P_0 = stagnation pressure, psi, and
P_{atm} = atmospheric pressure, psi

(Sutton, 1992, p 55).

Substituting the specific heat ratio $\gamma = 1.226$ provided by Primex Industries for WAA90 propellant and assuming it to be representative of other propellants planned for testing in the vortex program permits the nozzle exit diameter to be calculated as a function of the orifice diameter and the propellant charge.

Table 11 indicates that a large inventory of nozzles is needed if vortex research is to explore a wide range of pressures. One approach is to assemble nozzles in segments, thereby enabling researchers to achieve variety by simply unscrewing parts and mixing different orifices. Another approach is to construct a single overexpanding nozzle and permit flow to separate naturally. As a starting point, a three-piece cone was precision machined (see fig. 18 and 19) on the electron deposition machine at the U.S. Army Armament Research, Development, and Engineering Center, Picatinny, NJ.

Table 11. Nozzle exit diameter calculated from eq (18) for a gas having $\gamma = 1.226$.

Stagnation pressure P_o (psi)	Inlet throat diameter, D^* (in.)		
	0.1875	0.25	0.50
100000	3.2	4.3	8.5
90000	3.1	4.1	8.2
80000	2.9	3.9	7.8
70000	2.8	3.7	7.4
60000	2.6	3.5	7.0
50000	2.4	3.2	6.5
40000	2.2	3.0	5.9
30000	2.0	2.7	5.3
20000	1.7	2.3	4.5
10000	1.3	1.7	3.5
5000	1.0	1.3	2.6

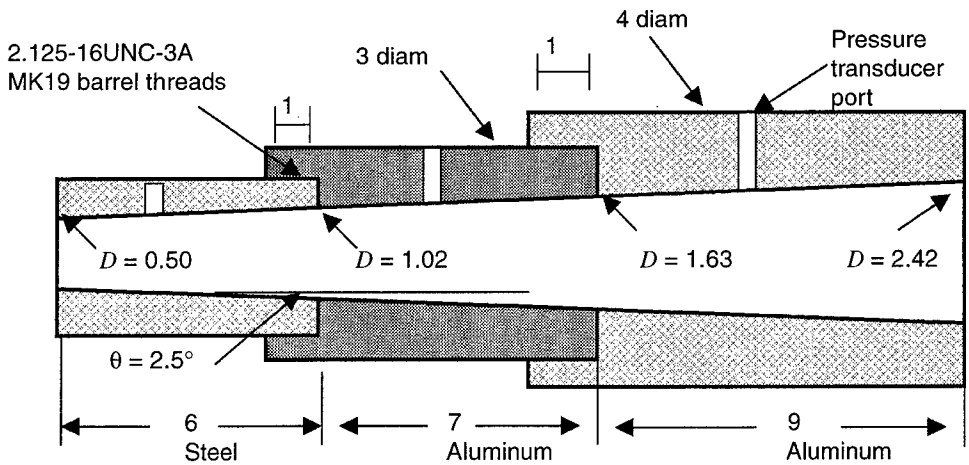

Figure 18. Variable-area nozzle design.

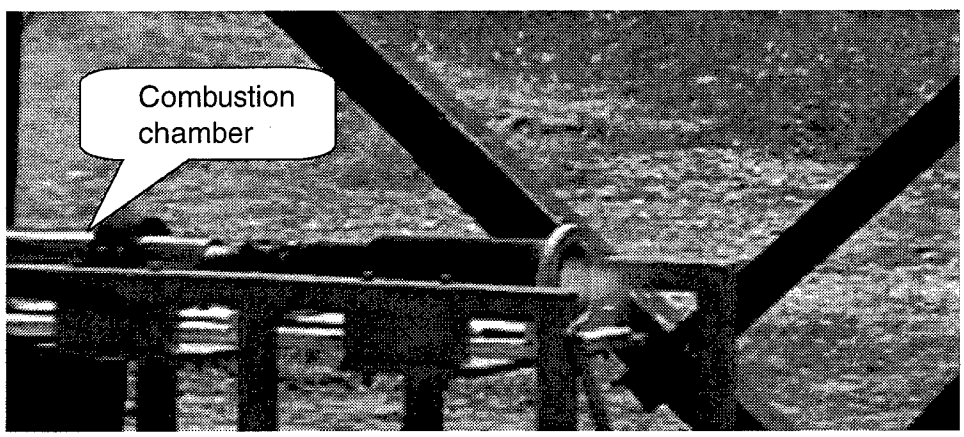

Figure 19. Experimental vortex ring generator with a three-stage variable-area nozzle.

The small 2.4-in. exit diameter was selected because combustion chamber pressures similar to those in blank cartridge fire in the MK19 can be administered. We selected the small cone angle for several reasons: first, a "fire-hose" jet stream has significant target knockdown capability; second, the front of the jet stream is more planar and therefore amenable to vortex formation; third, the resultant vortex is chest size and therefore more capable of total agent transfer onto a target; and last, the burning propellant adds heat to the jet stream and a concern exists that velocity may be degraded if the expansion is more severe.

We performed simple exploratory field tests by fitting the 2.4-in. nozzle sequentially with 3⁄16-, ¼-, and ½-in. throat diameters and subjecting it to firings of 12 and 24 g of smokeless powder. These combinations of nozzle diameters are designed to expand 50, 20, and 5 kpsi to atmospheric pressure. One intent of the test was to compare the actual shapes of muzzle blasts recorded on video to the design expectations.

For example, a fully expanded flow with a fire hose appearance occurs when a combustion chamber pressure equals the design rating.

Underexpanded flow with a plume larger than the muzzle occurs if the pressure is too high. Further, overexpanded flow with a separated jet stream smaller than the nozzle occurs if the chamber pressure is too low. See figure 20.

Figure 20. Muzzle blast characteristics for various exhaust pressures.

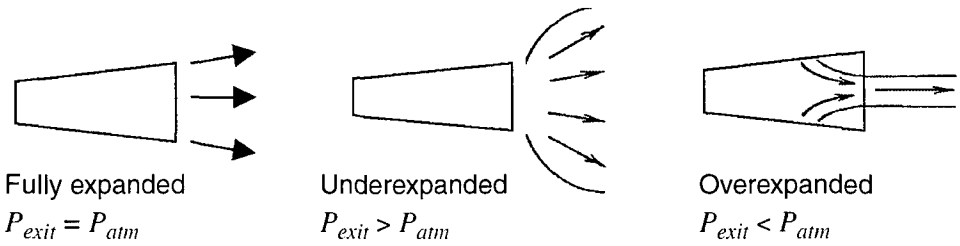

Results of test firings are summarized in figure 21. The pressure measurements in every instance were recorded by Kistler 607C1 or 607C3 high-impedance transducers for 70- and 100-kpsi charges, respectively. Kistler 5010B1 dual-mode charge amplifiers and 1631 low-noise transducer cabling provided couplings to a Hi-Techniques 8-channel HT-6000 digital acquisition system. The statically calibrated transducers mounted in a 0.05-in. cavity have a rise time of 5 μs and a natural frequency of 66 kHz.

The combustion chamber with a 24-g charge generated peak pressures near 125, 90, and 50 kpsi. These significantly exceeded the 50-, 20-, and 5-kpsi pressures, which the nozzles were designed to expand to atmospheric. The implications are that the exit pressures should be high and the flow underexpanded. Video recordings of the muzzle blasts shown in figure 22 do show the large plumes typically associated with a Mach disk at the muzzle.

For the 12-g charges shown in figure 23, the peak pressures generated are 70, 50, and 30 kpsi, which are again higher than, but closer to, the nozzle design ratings of 50, 25, and 5 kpsi. The 3⁄16-in. throat is designed to expand 50 kpsi to atmospheric, yet inspection of the muzzle blast video from the 40-percent overcharge in figure 24 shows that the jet stream is fully expanded with minimal external burning. The ¼-in. throat driven by a 100-percent overpressure is also nearly fully expanded. Enlarged images from the muzzle blast video show only a mild Mach disk with little external burning. The ½-in. throat, on the other hand, is driven by a 600-percent overpressure, and this video displays a stronger Mach disk with greater external burning.

One impression we drew from these tests is that precision loading of propellant into the combustion chamber is not necessary to avoid Mach disks at the muzzle. Combustion chamber pressures exceeding the nozzle design by 50 percent may well produce fully expanded jet streams. A second impression is that the variable-area nozzle that uses 3⁄16- or ¼-in. orifices and 12-g charges is suitable to simulate vortex propagation from the MK19-3 platform. Finally, we conclude that a larger nozzle is needed for higher charges in the combustion chamber, and the equations used to design the variable-area nozzle appear to be reasonable for this task.

Pressure transducer readings near the exit of the nozzle are summarized in figure 25. When relative shapes are compared to one another rather than absolute values, we draw the same conclusions about the quality of the muzzle blasts. As a result, the complexity of gathering pressure transducer data may be unnecessary. Visual observations through slow-motion camcorder recordings may be sufficient.

Figure 21. Midpoint combustion chamber pressures generated with 24 g WST1 propellant detonated by an M17 squib through a ½-in.-diam 0.02 BeCu rupture disk, a 2.4-in. nozzle exit diam, and various throat diameters.

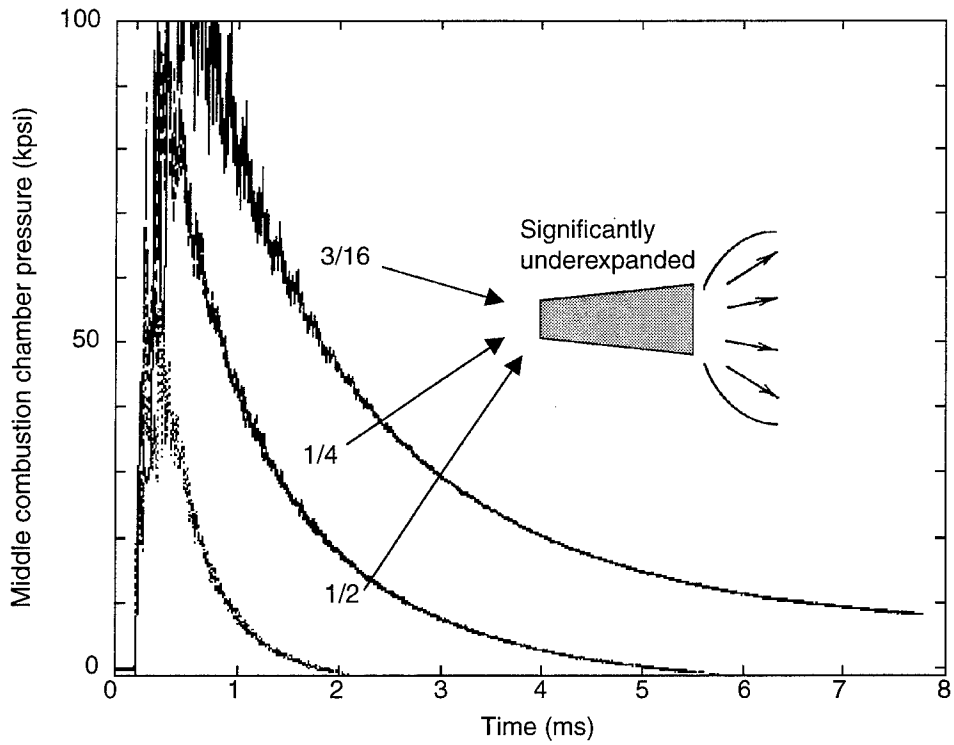

Figure 22. Camcorder images of 24-g WST1 smokeless powder firings show Mach disks at muzzle of variable-area nozzle. Camera angles and positions varied between shots, so care must be used when images are compared.

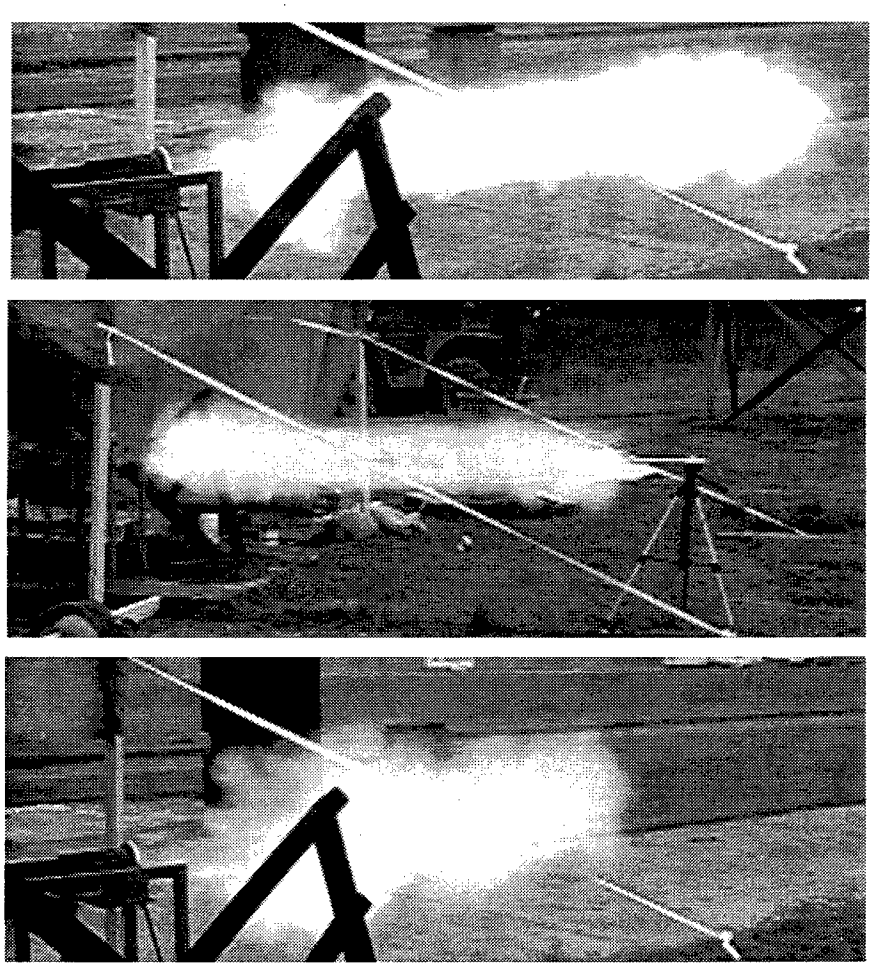

Figure 23. Midpoint combustion chamber pressures generated with 12 g WST1 propellant detonated by an M17 squib through a ½-in.-diam 0.02 BeCu rupture disk, a 2.4-in. nozzle exit diam, and various nozzle-throat diameters.

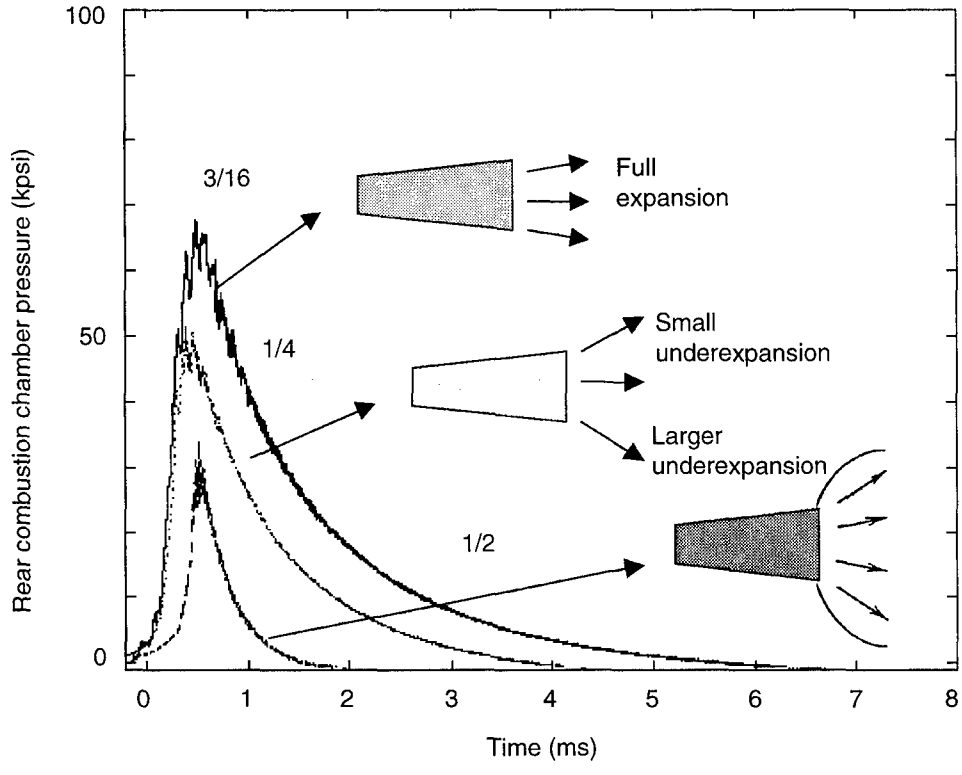

Figure 24. Camcorder images of 12-g WST1 smokeless powder firings showing smaller Mach disks than 24-g firings. Camera angles and positions are unchanged except for ½-in. firing, which is a frontal view.

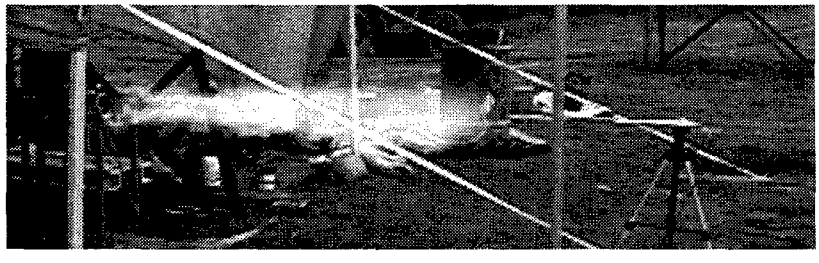

3/16-in. throat

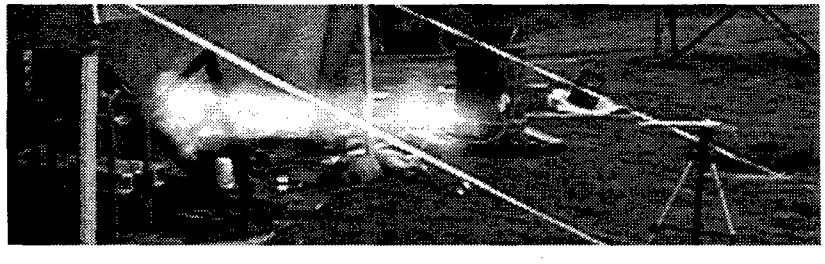

1/4-in. throat

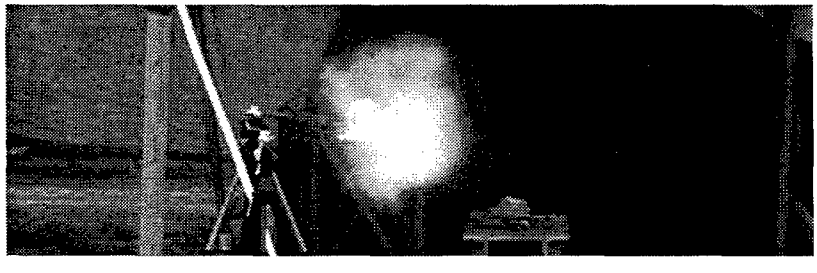

1/2-in. throat

Figure 25. Static pressures measured at wall of variable-area nozzle 2 in. before exit.

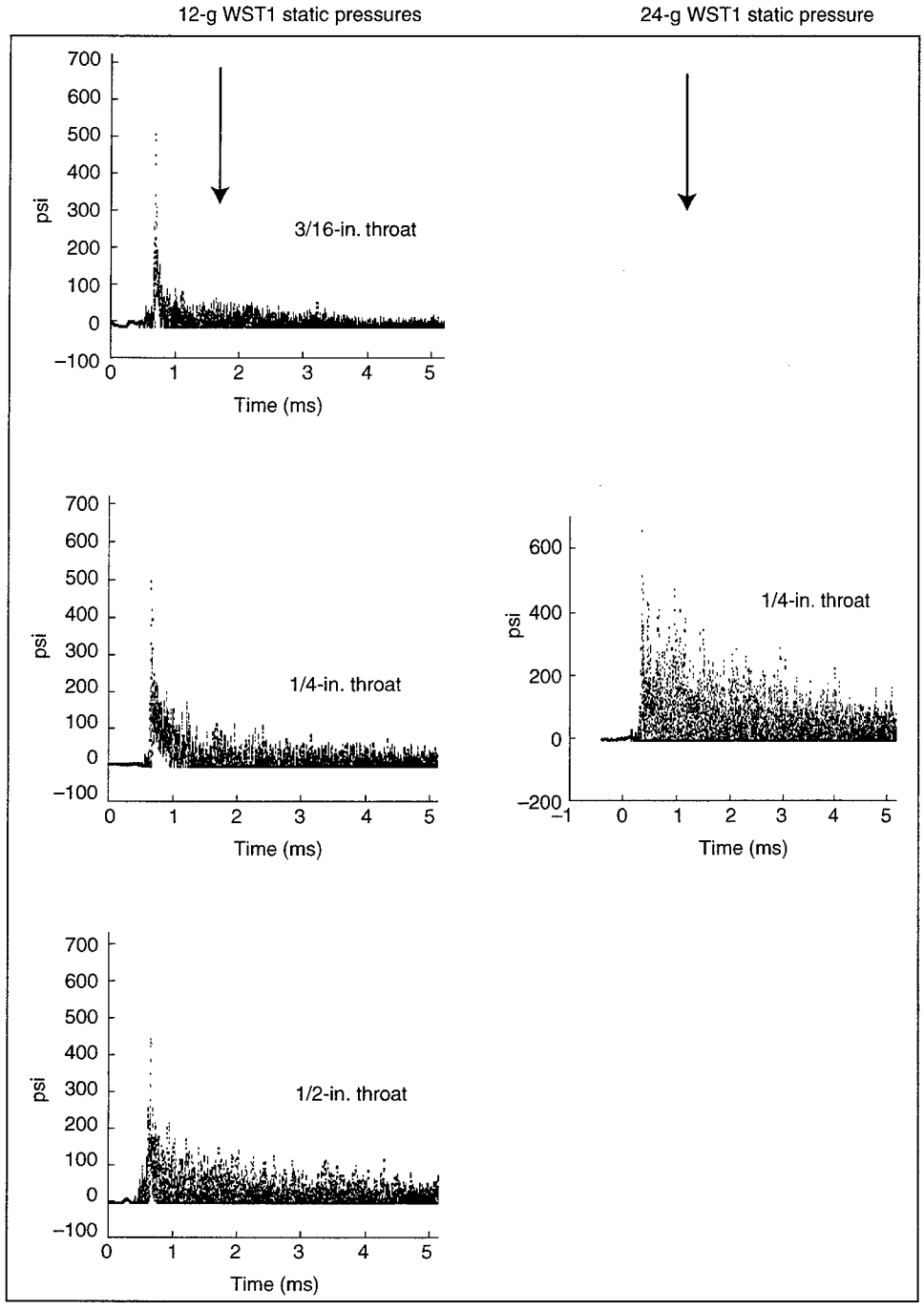

Because we expect that more powerful vortices with greater knockdown and range capabilities will be of interest for other weapons platforms, a nozzle with a larger exit diameter is sketched in figure 26. The most significant changes are an increase in divergence angle to reduce length and a change to plastic to reduce weight.

The steel section connects to the gas generator coupling (a design of this type of pressure chamber was described in previous sections of this report). To design the plastic cone, the pressure distribution must be defined and the resulting hoop stresses calculated for comparison to the

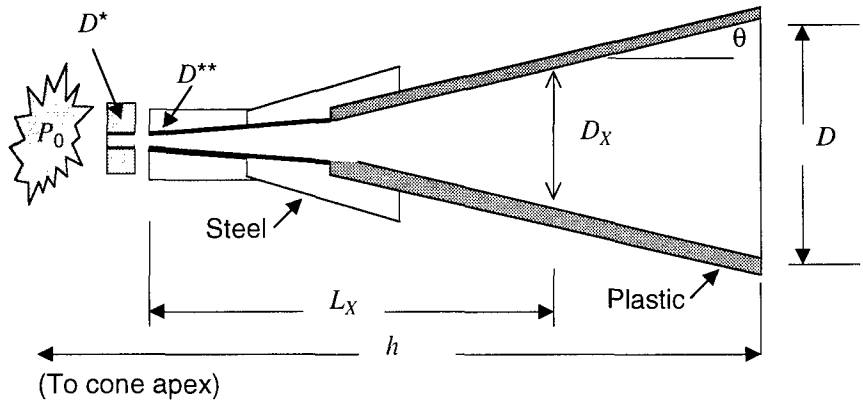

Figure 26. Assembly view of an overexpanding nozzle.

material strength. The pressure P_x at any diameter D_x may be estimated from

$$\left[\frac{D^*}{D_x}\right]^2 = \left[\frac{\gamma+1}{2}\right]^{1/(\gamma-1)} \left[\frac{P_x}{P_0}\right]^{1/\gamma} \sqrt{\frac{\gamma+1}{\gamma-1}\left[1-\left(\frac{P_x}{P_0}\right)^{(\gamma-1/\gamma)}\right]} \quad . \tag{19}$$

And geometry shows that the position L_x of the diameter is given by

$$D_x = D^* + 2L_x \tan\theta \, . \tag{20}$$

Solving the equations for any of the stagnation pressures or throat diameters authorized for the vortex ring gun shows that a dramatic pressure drop occurs in the first few inches, and use of a thin plastic or aluminum cone in the lower pressure zone is therefore reasonable. By treating the thin cone as a membrane without support from internal shearing stresses and by approximating pressure within the cone as a linear distribution, we can approximate a worst-case hoop stress at the steel-plastic interface by

$$\sigma_{max} = \frac{\beta h^2 \tan\theta}{4t\cos\theta} \, , \tag{21}$$

where

β = cone pressure gradient, lb/in.^{3},
h = cone length to vertex, in.,
θ = cone half angle, deg, and
t = cone thickness at bolts, in.

(Faupel, 1964, pp 225–227).

The composite nozzle in figure 27 was designed and fabricated in cooperation with EWS Ltd. Worst-case stress analysis indicated that hoop stresses were less than 6000 psi, so the design was released for field test. The assembly was subjected to more than 100 test firings at a variety of pressures without thermal or mechanical failures.

Figure 27. Overexpanding nozzle design.

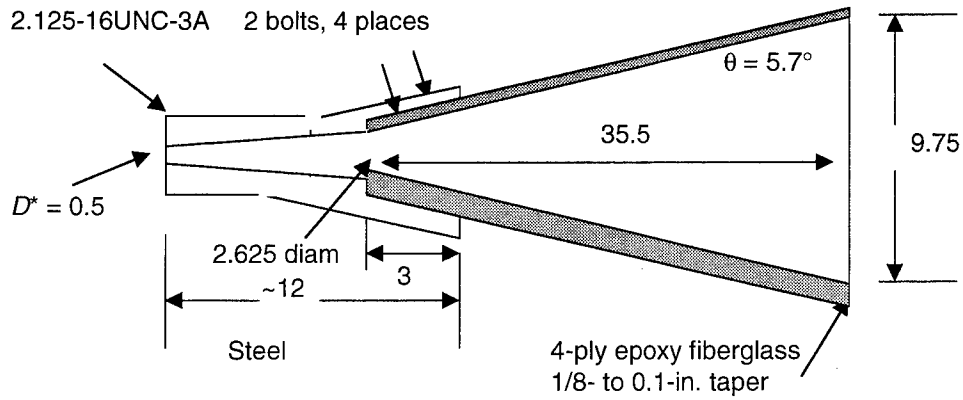

The disadvantage of this nozzle design is the larger dispersion angle used to shorten the length to a 10-in. outlet diam. A fire-hose-style exhaust is needed, so we attached an extension tube to straighten flow and mitigate the effects of external burning by using a 10-in., 4-ft-long, 165-psi polyvinyl chloride water pipe. Figures 28 and 29 show that a trombone-style mounting allows adjustments in length and tilting for minor corrections in aim.

In this configuration the nozzle operates at the maximum conditions specified for the combustion chamber. By simply changing the diameter of the extension tube, we can also use the nozzle to fully expand shorter duration and lower magnitude pulses that ordinarily require an inventory of cones of different area ratios (outlet to throat). The concepts behind the universal nozzle are presented below.

Figure 30 shows that if the extension tube is removed and a lower charge is fired in the combustion chamber, overexpansion will occur in the diverging nozzle, i.e., static pressures inside the nozzle will fall below atmospheric. The flow of propellant will separate from the wall and oblique shocks will form at the point of separation. The net result is that the jet stream will emerge at atmospheric pressure, but at a lower velocity. Unlike the flow through a Mach disk, the jet stream remains supersonic and emerges at a smaller diameter than that of the exit of the nozzle (Sutton, 1992, pp 63–67).

Figure 31 illustrates the premise that placing a pipe of the proper diameter in the cone will reduce the nozzle area ratio, mitigate the overexpansion, reduce external burning, and straighten the flow.

Two concerns are (1) shock waves emanating from the leading edge of the tube that may degrade the jet stream and (2) the means to select the proper diameter tube. Shock assessment is made by field tests. Three means are available to correlate tube diameters to combustion chamber charges: (1) position pressure transducers along the length of the cone, (2) perform computer modeling, and (3) conduct empirical tests using video cameras. The latter two were used at ARL, and the computer modeling is described below.

Figure 28. Assembly view of an over-expanding nozzle with an adjustable extension to straighten flow.

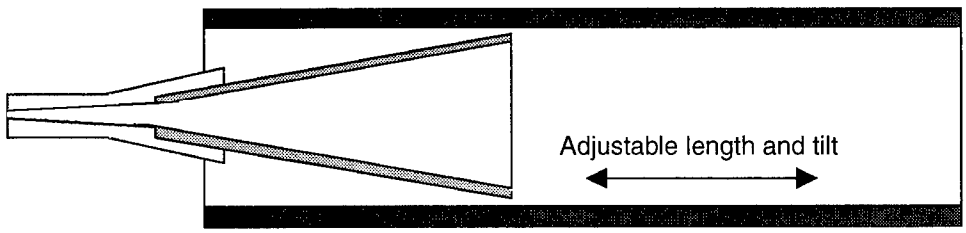

Figure 29. Side and rear view of universal vortex ring generator and extension tube mounted inside a protective shelter.

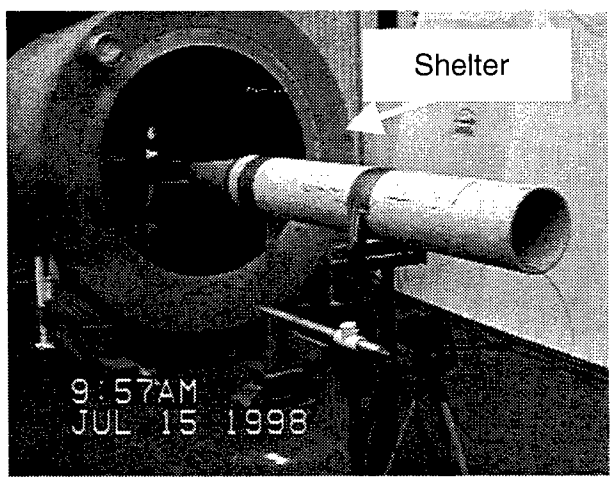

The modeling used in this report was done with the Adaptive Research CFD2000 computational fluid dynamics software; calculations were done on both the Cray and a desktop dual-Pentium PC. Input data are shown in figure 32, and initial conditions were the combustion properties for the WAA90 propellant. The surrounding environment was assumed to be the same gas as the propellant, but at ambient temperature and pressure.

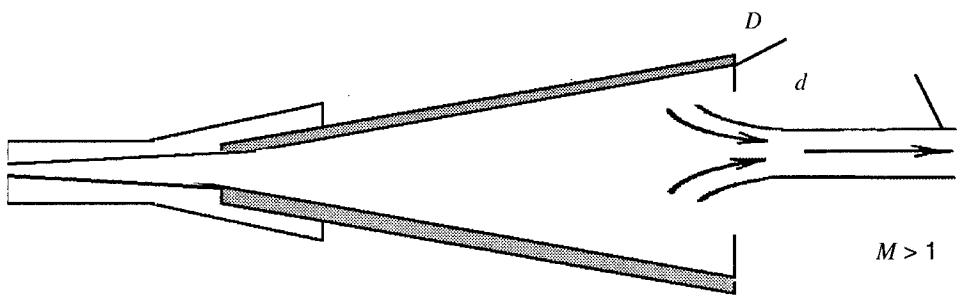

Figure 30. Jet stream separation from wall of an overexpanding nozzle.

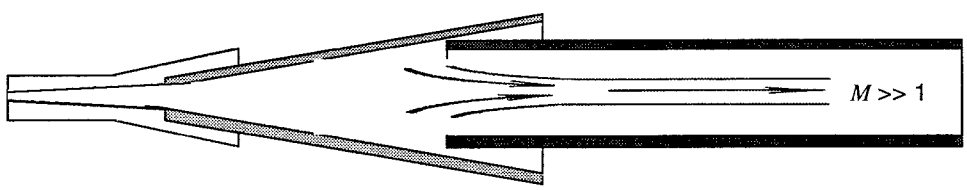

Figure 31. Concept for adjusting exit diameter of an overexpanding nozzle.

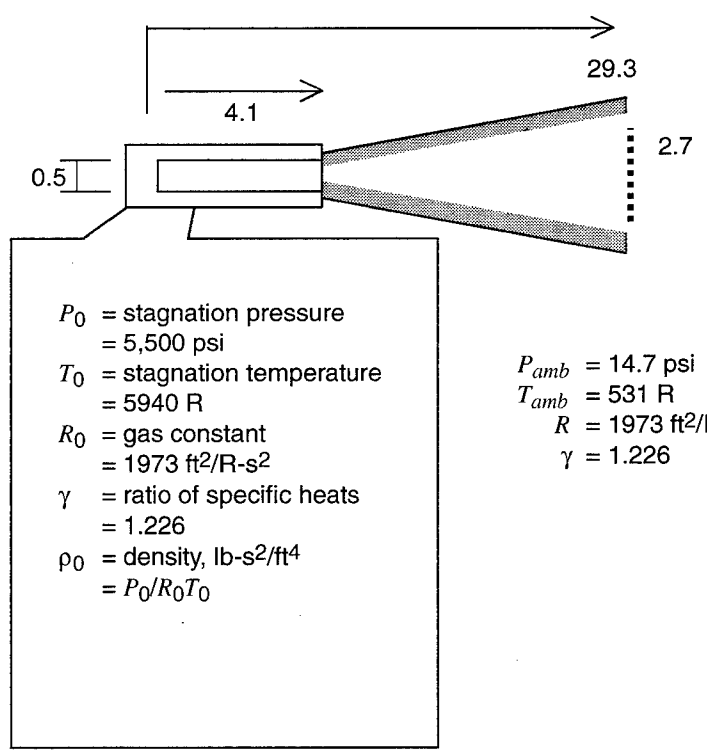

Figure 32. Schematic of an overexpanding nozzle subjected to transient flow analysis using Adaptive Research CFD2000 software.

Figure 33 shows that a sudden release of pressure at the orifice propagates a shock down the centerline of the nozzle, but flow behind the shock is not steady state because of rapidly decaying pressure in the combustion chamber.

At 0.45 ms, the pressure behind the shock is atmospheric. This occurs at 19.8 in. where the diameter is 1.87 in. See figures 34 and 35. A flow-straightening tube of this diameter must be inserted into the nozzle.

Note that if the combustion chamber pressure had not decayed with time, fully expanded flow would have required a much larger nozzle. Nozzle design for small charges and less energetic propellants requires computer modeling.

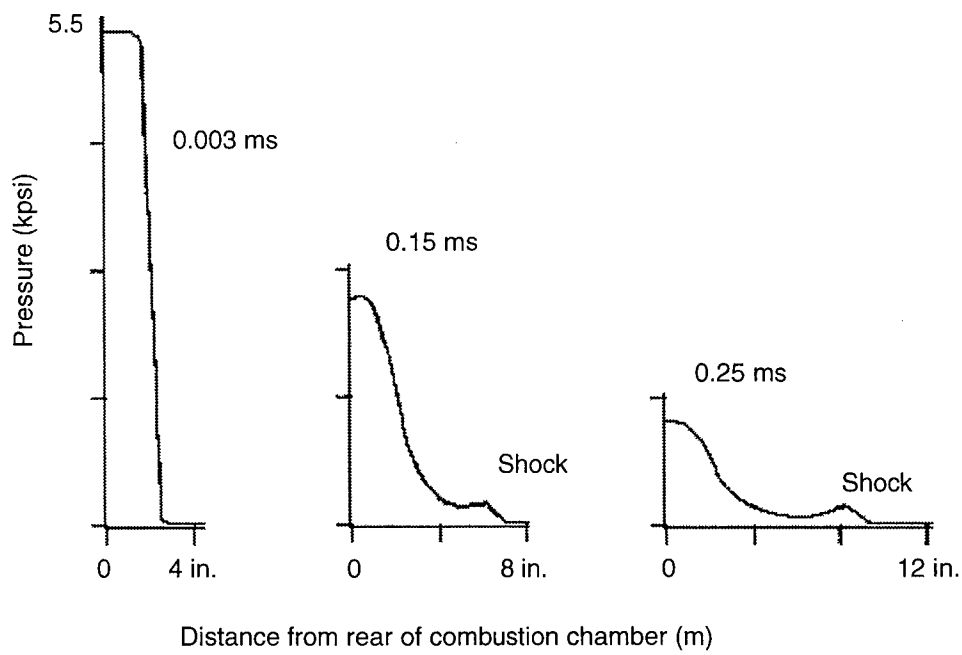

Figure 33. Unsteady flow resulting from a small charge in combustion chamber.

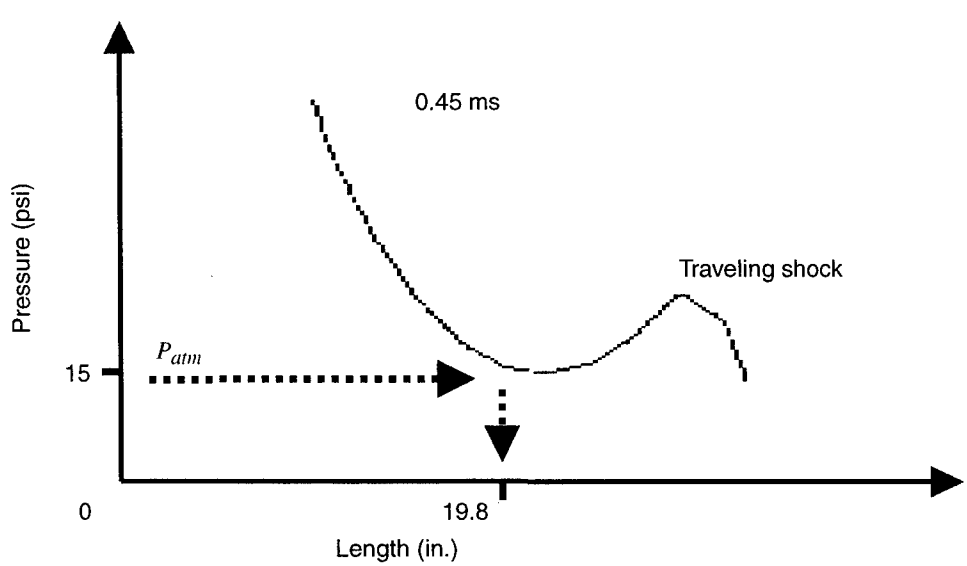

Figure 34. Computer technique for selecting a nozzle length.

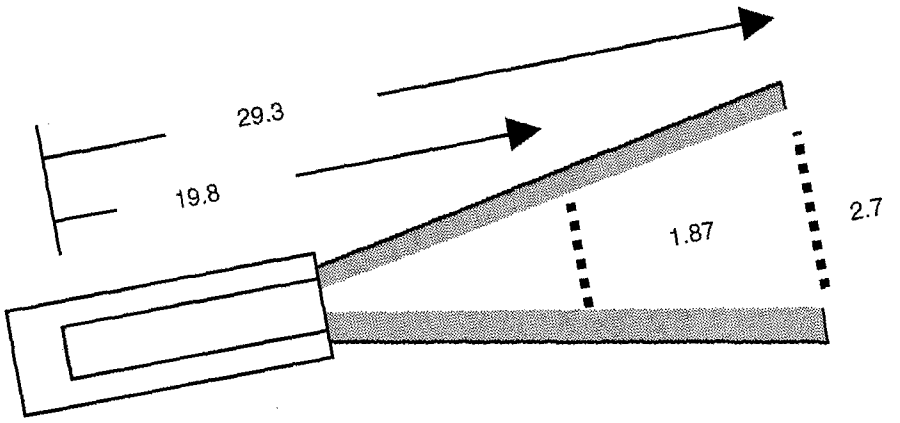

Figure 35.
Comparison of nozzle sizes for long- and short-duration pulses.

4. Agent Injection

The vortex ring is being designed in part to transport incapacitating irritants, malodors, and marker dyes to select targets in a crowd. Two concerns are leakage from the muzzle blast onto the operators and leakage from the vortex onto personnel below the flight path. One design guideline is to select compound agents that require spin mixing in flight and activate only upon arrival at the target.* A second design guideline is to use gaseous agents (rather than aerosols) that will resist ejection by centrifugal forces in the spinning vortex.

The intent is to store unmixed binary agents in the nozzle and inject the individual components sequentially into the jet stream. The properties of the jet stream during gunfire and of the vortex during flight must accordingly be estimated to select agents that can not only resist the thermal pulse but also provide an effective concentration at the target. The jet stream properties are also needed to select the location of the injection (i.e., boundary layer or main stream) and to design the injection mechanism. A number of materials are currently used as agents for crowd control, and others such as cortyl mercaptan (skunk scent) should be considered as candidates. Hardware and software are currently unavailable for screening, but an initial assessment of the suitability for jet stream injection can be made with the steady-state rocket engine equations compiled in figure 36.

Discussions on mixing in liquid vortices are presented by Johart (1995).

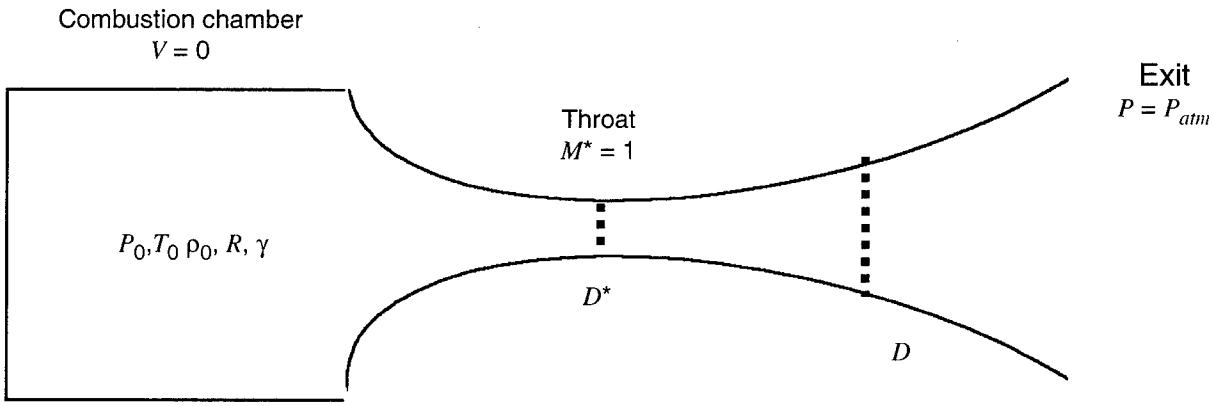

Gas properties are provided by the powder manufacturer

$$P^* = P_0\left[\frac{2}{\gamma+1}\right]^{\gamma/\gamma-1} \qquad M = \sqrt{\frac{2}{\gamma-1}\left\{\left(\frac{P_0}{P}\right)^{\gamma-1/\gamma} - 1\right\}}$$

$$\rho^* = \rho_0\left[\frac{2}{\gamma+1}\right]^{1/\gamma-1} \qquad \rho = \rho_0\left[\frac{T_0}{T}\right]^{\gamma/\gamma-1}$$

$$T^* = T_0\left[\frac{2}{\gamma+1}\right] \qquad T = \frac{T_0}{1+\frac{\gamma-1}{2}M^2}$$

$$C^* = \sqrt{\gamma RT^*} \qquad C = \sqrt{\gamma RT}$$

$$V^* = C^*M^* \qquad V = CM$$

$$\dot{\omega} = \rho^*A^*V^* \qquad D = D^*\sqrt{\frac{1}{M}\left[\frac{2}{\gamma+1}\left(1+\frac{\gamma-1}{2}M^2\right)\right]^{\gamma+1/2(\gamma-1)}}$$

M = Mach number
ρ = density, lb-s^2/ft^4
T = temperature, R
C = sound speed, ft/s
V = velocity, ft/s
D = diameter, ft
R = gas constant, ft^2/R-s^2
γ = ratio of specific heats
$\dot{\omega}$ = weight rate of flow, lb/s

Figure 36. Design equations for steady, isentropic, adiabatic, and supersonic flow.

5. Vortex Detection

Some of the program objectives are to optimize the physical parameters of the vortex as required to knock down targets at close range, mix compounds of incapacitating agents while in flight, transport these agents to targets in reasonable concentrations, resist shattering in wind gusts, and resist dispersion in crosswinds.

The physical parameters critical to control for optimum vortex ring performance at the target are unknown, so we used a number of vortex visualization techniques. Figure 37 shows that for simple confirmation of the presence of a vortex, the use of powders with a smoke residue, as well as a Panasonic camcorder with playback, stop action, PC compatibility, and shutter speeds to 0.1 ms, is adequate.

Figure 38 shows that a shallow, 12-in. line of colored powdered chalk poured into the nozzle near the muzzle enables the camcorder to track the path of vortices formed from smokeless powder up to 50 ft.

Figure 39 shows that the acoustic signature of gunfire coupled with target impact may be used to record the average vortex velocity. Spectral analyses of the audible whistle emitted by the vortex flying overhead is being considered as a possible gauge of the vortex spin.* For more scientific measures of the vortex formation from jet streams higher than Mach 3, a smaller generator is planned for use in the 9-ft Schlieren facilities at the Pennsylvania State University.

To assess the setup conditions of the prototype vortex generator hardware, we had to gauge only the vortex shape, size, and dispersion, and we did this using the digital mechanical target shown in figure 40, a Panasonic video camera, and a Snappy frame grabber for transferring data to the desktop computer.

This target is nylon net of 1.25-in. squares supporting 350 independent pendulums. The pendulums are Diamond brand wooden, spring-loaded clothespins painted different colors front and back. Each is mounted to be free to swing backward and slide sideways, but unable to rotate beyond 180 deg. A qualitative gauge of the vortex strength from shot to shot is the distance dislodged pendulums are thrown downrange. The best results to date have been displacements of 80 ft.

Figure 41 shows that a quantitative gauge of the vortex momentum is obtained by positioning a standardized mannequin immediately behind the digital target and adjusting the weight between 50 and 250 lb until knockdown is achieved. The mannequin used in the early phase of the ring vortex program is the easiest to knock down; it is a lock-kneed, 6-ft-tall, wooden E-silhouette with a 2- by 1.5-ft chest, a 36-in. center of gravity, and a 12-in. shoe with the ankle at mid-foot. Ground support is provided by a flat plywood board.

Analyses of such sound effects are discussed by Zaitsev and Kopev (November–December 1993).

Figure 37. A 2-ft-diam, smoke-filled vortex ring at muzzle of generator.

Figure 38. A chalk-filled vortex ring impacting a mannequin at 30 ft.

Figure 39. Acoustic signature of a ring vortex approaching and impacting a plastic target. Microphone was positioned at 50 ft and target was 120 ft downrange.

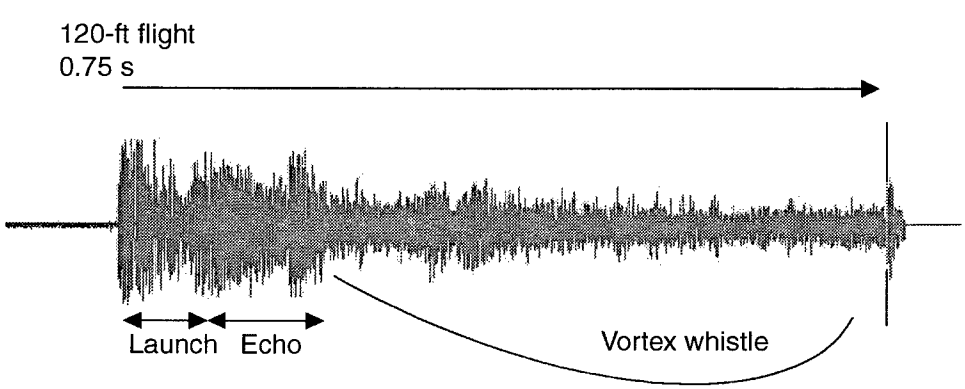

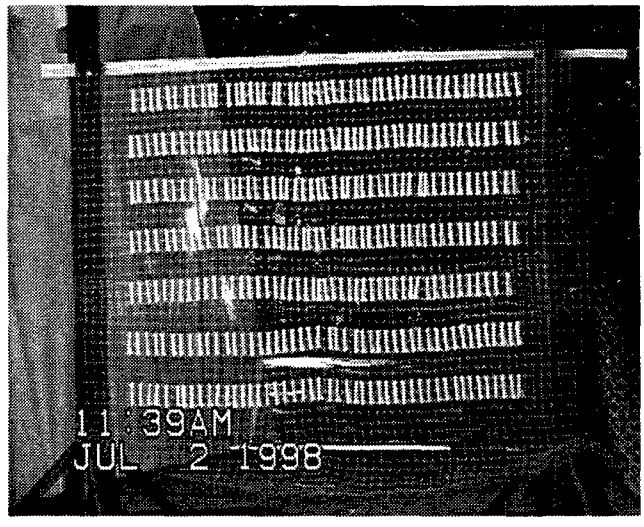

Figure 40. Digital mechanical target for measuring vortex size, shape, dispersion, and strength.

Figure 41. Technique used to gauge generator's strength and dispersion.

To inquire about videos and soundtracks, contact glucey@erols.com.

Of particular interest are the size, weight, and volume of aerosols that can be retained in the vortex core without being shed by centrifugal forces. One planned approach to these data was to fire vortices into cold air and use Schlieren or shadow-graph techniques to monitor the water condensation that forms naturally. Figures 42(a), (b), and (c) illustrate an example wherein a vortex is generated by an exploding oxygen bottle in the cockpit of a burning B29 in the Arctic. The heavy oil-laden smoke is seen to be transported a distance roughly equal to the length of the plane. The core of the vortex remains visible much farther downrange and is believed to be condensation.

Figure 42(a). An oily smoke-laden vortex launched in NNE direction from a cockpit window of a burning B29 (courtesy Nova TV).

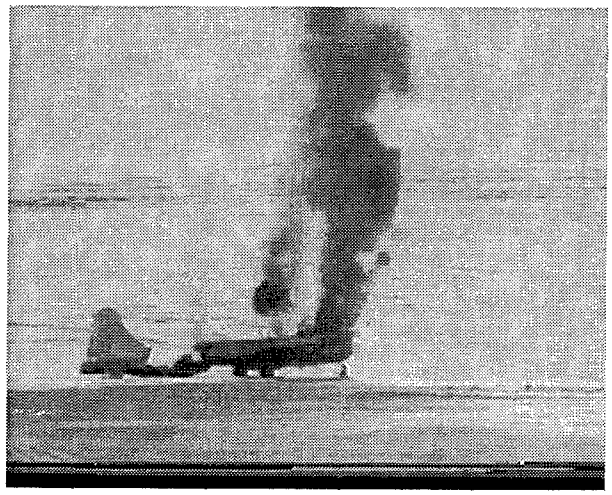

Figure 42(b). Vortex progressing a distance equal to length of aircraft while still retaining a residue of smoke aerosol.

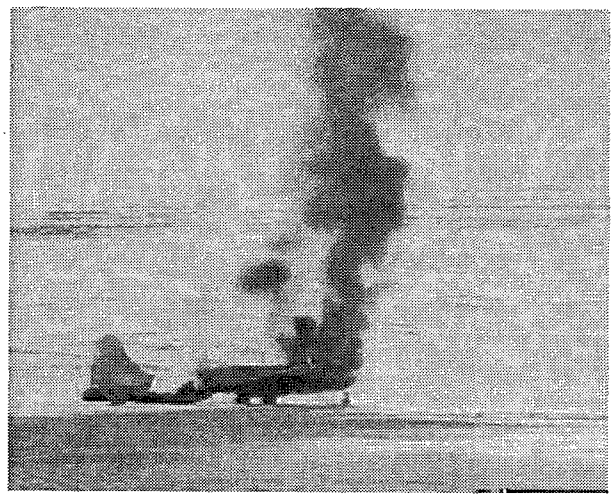

Figure 42(c). Vortex ring well downrange of aircraft. White coloring is believed to be moisture condensation within spinning low-pressure core.

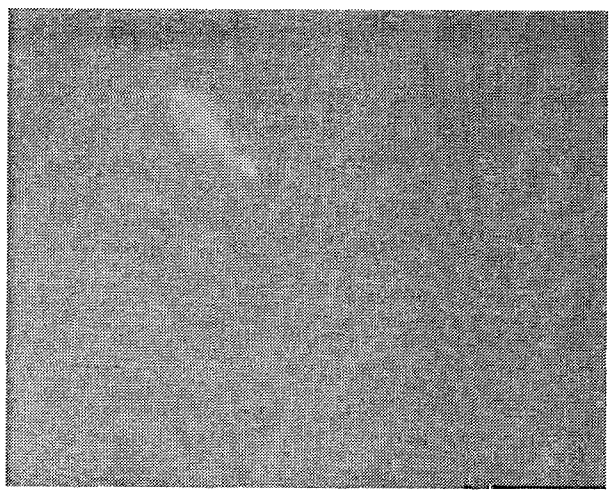

6. Discussion and Recommendations

One of the missions of the vortex ring generator program is to provide target knockdown by means of momentum transfer. The vortex momentum is comprised of axial and angular components, and equations correlating the velocities to the interior ballistics of the generator are unavailable in the literature. Further, equations showing the variations of vortex spin with range are sparse. Also, there is a technology gap in the axial velocity equations often expressed as

$$V = f(V_0 / X^n) , \tag{22}$$

where

V = instantaneous velocity, ft/s,
V_0 = launch velocity, ft/s,
X = displacement, ft, and
n = constant.

This expression works well for incompressible fluids where the launch velocity is identical to that of the driving piston. The launch velocity for vortices generated by supersonic jet streams is unknown, however, and its determination requires developing a better understanding of the mechanisms of formation.

An outline of the concepts being explored at ARL is presented in the following paragraphs as a guide for future experiments with the high-pressure generator.

When an explosive initiates in a straight barrel, three events significant to vortex formation occur. Figure 43 shows that a blast-shock expands spherically from the muzzle; an underexpanded jet stream emerges at a high Mach number; and a stationary normal shock (Mach disk) that forms at the muzzle adjusts the static pressure to atmospheric and degrades the jet stream to a Mach number below 1 in a turbulent plume.

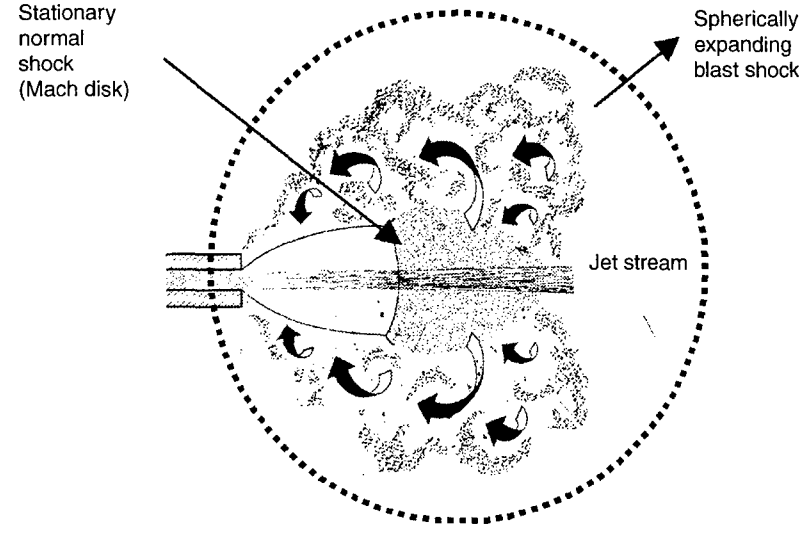

Figure 43. Typical gunfire muzzle blast.

This type of vortex ring generator has been studied by designers in Germany, Russia, and the United States, but we could not find a record of successful weapons fielding. One reason may be inefficiency, i.e., unacceptable size and weight of a weapon required to achieve reasonable range and agent transport capacity.*

ARL hypothesizes that the Mach disk may have limited the previous investigators by severely degrading the jet stream velocity downstream from the shock. A concept was advanced to eliminate the Mach disk using a diverging nozzle to fully expand gas to near atmospheric pressures, as shown in figure 44. A prototype gas generator was constructed with the capability to operate at high stagnation pressures. This feature enabled vortices to be launched with both high density and high velocity.

To reduce run-time and better understand the mechanisms of vortex formation, one can exclude the gun and nozzle from computer models. The jet stream is simply presented as a cylindrical gas bullet with a weight equal to the unexploded powder and an initial temperature, density, and velocity identical to those that would be achieved upon exit from a supersonic nozzle.

The simulation in figure 45 shows drag slowing the velocity of the tip and initiating a radial expansion that is in turn confined by the back pressure of the blast-shock. A rearward curling action evolves as the remnants of the faster moving cylinder fill the spherically expanding blast-shock. Part of this redirected flow is lost into the atmosphere, and part reenters the jet stream to form a spinning, translating torus once the low-pressure wake at the stern of the cylinder arrives at the high-pressure shock. At this time the shock detaches from the tip, whereupon the torus slows and transforms into two ring vortices: a subsonic vortex launched at the target and a slow vortex lingering at the muzzle.

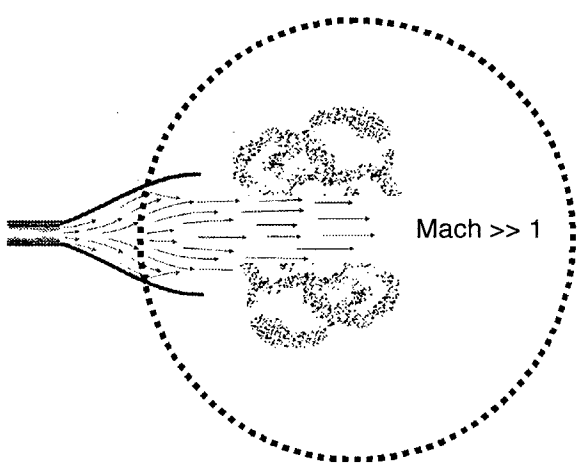

Figure 44. Laval nozzle expanding a propellant to atmospheric pressure without a Mach disk.

A comprehensive empirical study of vortex propagation in a military environment is summarized by Spice (1955, 1956).

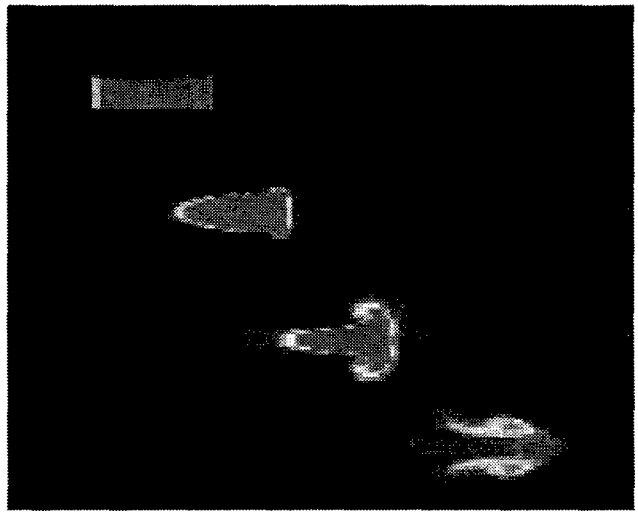

Figure 45. Computer simulation of a supersonic gas "bullet" rolling up into two subsonic ring vortices.

Figure 46 is a schematic of the critical parameters described in figure 45. The prototype vortex ring generator is expected to be a critical tool for demonstrating the parameters shown and then for empirically deriving both axial and angular equations of motion of the launch vortex. These equations are considered essential for optimizing the knockdown and agent transport capabilities of a vortex at distant targets.

The prototype vortex ring generator is also expected to be useful for developing the techniques and timing for injecting agents into the jet stream, assessing losses at the gunsite and in flight, and assessing the effects of wind gusts and crosswinds on vortex dispersion.

As currently designed, the prototype breech-loading vortex ring generator is suitable for 5 shots per hour at 75 kpsi when changes in the throat diameter, rupture disk, and breech plug are required operating conditions. The firing could be increased to 10 shots per hour and 100 kpsi if only the breech plug needs to be operational. The pressure limitation is due to the tendency of the coupling threads to distort and require rework after each firing.

Recommendations for future users follow:

(1) Reexamine the use of rupture disks as a means of improving the reliability of vortex generation.

(2) Always inspect the combustion chamber externally after each firing for deformations and cracks, and establish a routine inspection cycle for assessing the internal condition.

(3) Use 4340 Rc 29 steel for the combustion chamber and the coupling.

(4) Redesign the coupling for higher load-bearing buttress threads.

(5) Design the breech plug to eliminate the feed-through hole for the detonator wires.

(6) Refer technical questions to the cooperative team members listed in figure 47.

Figure 46. Schematic of three stages of vortex formation: firing, roll-up, and launch.

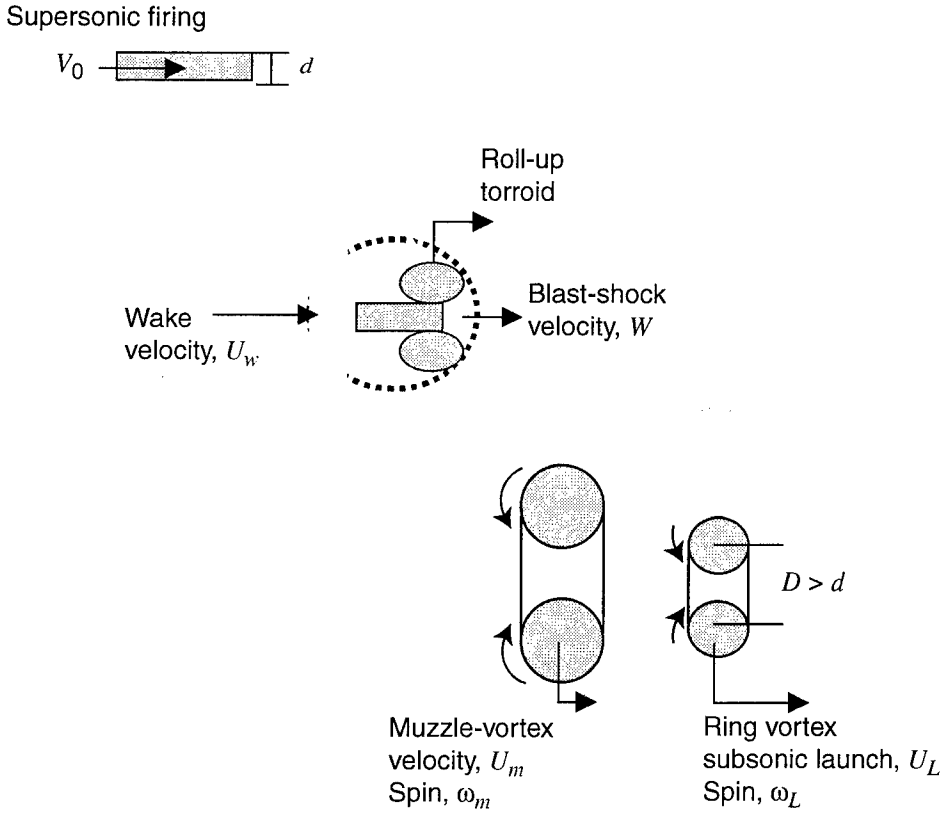

To inquire about results of computer models available on CD-ROM, contact glucey@erols.com.

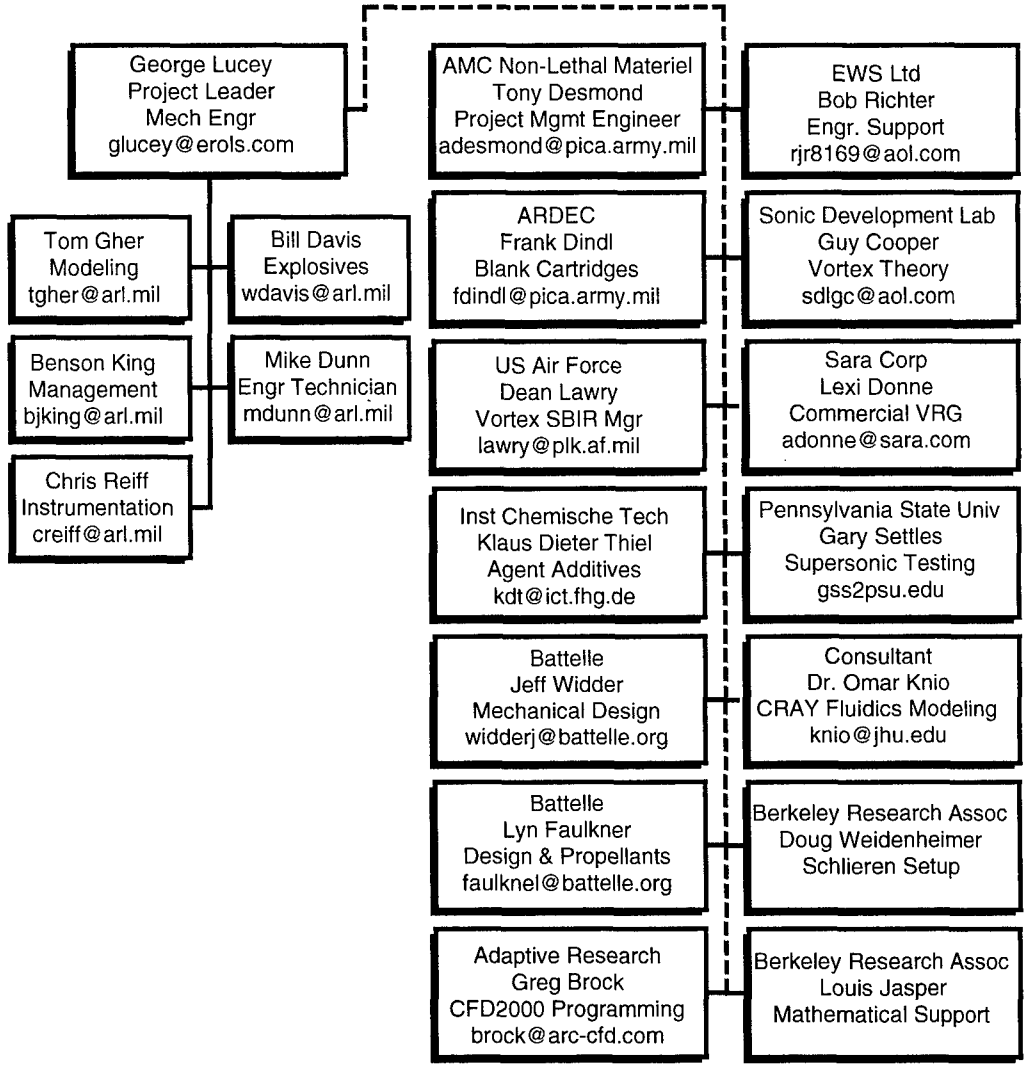

Figure 47. ARL vortex ring generator cooperative, 24 February 1999.

References

Baxivanos, V. (n.d.), Final Report on Methodology Investigation of Setback and Spin for Artillery, Mortar, Recoilless Rifle, and Tank Ammunition, TECOM Project No. 7-CO-P86-AP3-002, Report No. USACSTA-6709.

Blake, A. (1986), *Design of Mechanical Joints*, Marcel Dekker, Inc., NY, pp 379–383.

Faupel, J. (1964), *Engineering Design*, Wiley & Sons, NY.

Green, R., ed. (1996), *Machinery's Handbook*, 25th ed., Industrial Press, pp 1416 and 1640.

Johart, H. (1995), "Chemically reactive turbulent vortex rings," *Phys. Fluids* **10** (October), pp 2420–2427.

Spice, R. (1955, 1956), "A Study of Vortex Rings in Air," *Aerojet-General*, Report 1030, Contract NONR-1498(00) (26 October 1955) and Report 1210 (24 December 1956).

Sutton, G. P. (1992), *Rocket Propulsion Elements*, 6th ed., Wiley & Sons, NY.

Tapley, B., ed. (1990), *Eshback's Handbook of Engineering Fundamentals*, 4th ed., Wiley & Sons, table 16-14.

Zaitsev, M., and V. Kopex (1993), "Mechanism of sound radiation by a turbulent vortex ring," *Acoust. Phys.* **39**, 6 (November–December).

Distribution

Admnstr
Defns Techl Info Ctr
Attn DTIC-OCP
8725 John J Kingman Rd Ste 0944
FT Belvoir VA 22060-6218

Ofc of the Secy of Defns
Attn ODDRE (R&AT)
The Pentagon
Washington DC 20301-3080

OSD
Attn OUSD(A&T)/ODDR&E(R) R J Trew
Washington DC 20301-7100

AMCOM MRDEC
Attn AMSMI-RD W C McCorkle
Redstone Arsenal AL 35898-5240

CECOM
Attn PM GPS COL S Young
FT Monmouth NJ 07703

Dir for MANPRINT
Ofc of the Deputy Chief of Staff for Prsnnl
Attn J Hiller
The Pentagon Rm 2C733
Washington DC 20301-0300

Joint Non-Lethal Weapons Directorate
Attn J Busic (5 copies)
3097 Range Rd
Quantico VA 22134-5100

TACOM/ARDEC
Attn AMSTA-AR-CCL-E H Moore (5 copies)
Bldg 79
Picatinny Arsenal NJ 07806-5000

TECOM
Attn AMSTE-CL
Aberdeen Proving Ground MD 21005-5057

US Army Armament Rsrch Dev & Engrg Ctr
Attn AMSTA-AR-CCL-E F Dindl (2 copies)
Bldg 7
Picatinny Arsenal NJ 07806-5000

US Army Armament Rsrch Dev & Engrg Ctr
Attn AMSTA-AR-TD M Fisette
Bldg 1
Picatinny Arsenal NJ 07806-5000

US Army Edgewood RDEC
Attn SCBRD-TD G Resnick
Aberdeen Proving Ground MD 21010-5423

US Army Info Sys Engrg Cmnd
Attn ASQB-OTD F Jenia
FT Huachuca AZ 85613-5300

US Army Natick RDEC Acting Techl Dir
Attn SSCNC-T P Brandler
Natick MA 01760-5002

US Army Simulation, Train, & Instrmntn Cmnd
Attn J Stahl
12350 Research Parkway
Orlando FL 32826-3726

US Army Tank-Automtv Cmnd Rsrch, Dev, & Engrg Ctr
Attn AMSTA-TA J Chapin
Warren MI 48397-5000

US Army Train & Doctrine Cmnd
Battle Lab Integration & Techl Dirctrt
Attn ATCD-B J A Klevecz
FT Monroe VA 23651-5850

US Military Academy
Mathematical Sci Ctr of Excellence
Attn MDN-A LTC M D Phillips
Dept of Mathematical Sci Thayer Hall
West Point NY 10996-1786

Nav Surface Warfare Ctr
Attn Code B07 J Pennella
17320 Dahlgren Rd Bldg 1470 Rm 1101
Dahlgren VA 22448-5100

AFRL-DEOB
Attn D Lawry
3550 Aberdeen Ave SE
Kirtland AFB NM 87117-5776

Distribution (cont'd)

DARPA
Attn S Welby
3701 N Fairfax Dr
Arlington VA 22203-1714

Penn State University Gas Dynamics Lab
Attn G Settles
301D Reber Bldg
University Park PA 16802

Battelle Corp
Attn J Widder
2012 Tollgate Rd
Belair MD 21015

Battelle Corp
Attn L Faulkner (2 copies)
505 King Ave
Columbus OH 43201

Berkely Research Associates, Inc
Attn J Orens (2 copies)
5532 Hempstead Way
Springfield VA 22151

Delsys Corp
Attn C De Luca
PO Box 15734
Boston MA 02215

EWS Ltd
Attn R Richter (5 copies)
1430 Journey's End
Croton NY 10520

Hicks & Associates Inc
Attn G Singley III
1710 Goodrich Dr Ste 1300
McLean VA 22102

Institut Chemische Technologie
Attn K Thiel
Joseph-von-fraunhoferstr Pfinztal 7 D-75327
Germany

Palisades Inst for Rsrch Svc Inc
Attn E Carr
1745 Jefferson Davis Hwy Ste 500
Arlington VA 22202-3402

SARA Corp
Attn L Donne (2 copies)
15261 Connector LA
Huntington Beach CA 92649

Sonic Development Labs
Attn G Cooper (2 copies)
484 Rancho Dr
Ventura CA 93003

Army Rsrch Ofc
Attn AMSRL-RO-EN W Bach
PO Box 12211
Research Triangle Park NC 27709

US Army Rsrch Lab
Attn AMSRL-DD J Rocchio
Attn AMSRL-CM SGM J Tobiasz
Attn AMSRL-CI-LL Techl Lib (3 copies)
Attn AMSRL-CS-AS Mail & Records Mgmt
Attn AMSRL-CS-EA-TP Techl Pub (3 copies)
Attn AMSRL-CS-IS-PB W Davis
Attn AMSRL-CS-IS-SH S Rock
Attn AMSRL-CS-SE-DC M Dunn
Attn AMSRL-SE-D E Scannell
Attn AMSRL-SE-DE C Reiff
Attn AMSRL-SE-DS B King
Attn AMSRL-SE-DS G K Lucey (30 copies)
Attn AMSRL-SE-DS L Jasper
Attn AMSRL-SE-DS T Gher
Adelphi MD 20783-1197

REPORT DOCUMENTATION PAGE

Form Approved
OMB No. 0704-0188

1. AGENCY USE ONLY *(Leave blank)*	2. REPORT DATE	3. REPORT TYPE AND DATES COVERED
	December 1999	Final, FY98

4. TITLE AND SUBTITLE Vortex Ring Generator: Mechanical Engineering Design for 100-kpsi Operating Pressures

5. FUNDING NUMBERS
DA PR: A140
PE: 62120A

6. AUTHOR(S) George K. Lucey, Jr.

7. PERFORMING ORGANIZATION NAME(S) AND ADDRESS(ES)
U.S. Army Research Laboratory
Attn: AMSRL-SE-DS email: glucey@arl.mil
2800 Powder Mill Road
Adelphi, MD 20783-1197

8. PERFORMING ORGANIZATION REPORT NUMBER
ARL-TR-2096

9. SPONSORING/MONITORING AGENCY NAME(S) AND ADDRESS(ES)
U.S. Army Research Laboratory
2800 Powder Mill Road
Adelphi, MD 20783-1197

10. SPONSORING/MONITORING AGENCY REPORT NUMBER

11. SUPPLEMENTARY NOTES
ARL PR: 9NEYY1
AMS code: 622120.140

12a. DISTRIBUTION/AVAILABILITY STATEMENT Approved for public release; distribution unlimited.

12b. DISTRIBUTION CODE

13. ABSTRACT *(Maximum 200 words)*

Engineering design guidelines used to construct an explosive gas generator (100 kpsi maximum) and an adjustable area ratio (2844 maximum) nozzle are documented in this report. The equipment enables ring vortices to be generated using jet streams with significantly higher Mach numbers than previously reported in the literature. Studies are planned of the risks, limits, and capabilities of ring vortices for nonlethal crowd control applications. The focus is limited to 40-mm weapons, so this report is written to facilitate technology transfer to investigators interested in other applications and launch platforms.

14. SUBJECT TERMS
Vortex, ring vortex, nonlethal

15. NUMBER OF PAGES
52

16. PRICE CODE

17. SECURITY CLASSIFICATION OF REPORT	18. SECURITY CLASSIFICATION OF THIS PAGE	19. SECURITY CLASSIFICATION OF ABSTRACT	20. LIMITATION OF ABSTRACT
Unclassified	Unclassified	Unclassified	UL

NSN 7540-01-280-5500

Standard Form 298 (Rev. 2-89)
Prescribed by ANSI Std. Z39-18
298-102